

## Supporting Information

### **Mn-Rh Dual Single-Atom Catalyst for Inducing C–C Cleavage: Relay Catalysis Reversing Chemoselectivity in C- H Oxidation**

Chang-Jie Yang<sup>1,2</sup>, Yu-Da Huang<sup>2</sup>, Yu-Yuan Zhang<sup>2</sup>, Yong-Zhou Pan<sup>1</sup>, Jiarui Yang<sup>3</sup>,  
Ying-Ming Pan<sup>2</sup>, Tao Gan<sup>4</sup>, Hai-Tao Tang<sup>2\*</sup>, Xia Zhang,<sup>1</sup> Wen-Hao Li<sup>1\*</sup>, Dingsheng  
Wang<sup>3\*</sup>

<sup>1</sup>Department of Chemistry, Northeastern University, Shenyang, 110819, P. R. China

<sup>2</sup>State Key Laboratory for Chemistry and Molecular Engineering of Medicinal Resources, Key  
Laboratory for Chemistry and Molecular Engineering of Medicinal Resources (Ministry of Education of  
China), Collaborative Innovation Center for Guangxi Ethnic Medicine, School of Chemistry and  
Pharmaceutical Sciences, Guangxi Normal University, Guilin 541004, China.

<sup>3</sup>Department of Chemistry, Tsinghua University, Beijing 100084, China.

<sup>4</sup>Shanghai Synchrotron Radiation Facility, Shanghai Advanced Research Institute, Chinese Academy of  
Sciences, Shanghai 201204, China.

\*Correspondence to : liwenhao@mail.neu.edu.cn; httang@gxnu.edu.cn;  
wangdingsheng@tsinghua.edu.cn

## Contents

1. Reagents and Materials .....	3
2. Characterization .....	4
3. Computational method .....	4
4. Supplementary experimental section .....	6
5. $^1\text{H}$ , $^{13}\text{C}$ and $^{19}\text{F}$ NMR data of all products .....	54
6. Copies of $^1\text{H}$ , $^{13}\text{C}$ and $^{19}\text{F}$ NMR spectra for products .....	57
7. Supplementary References .....	67

## 1. Reagents and Materials

Unless otherwise noted, all reagents and solvents were obtained commercially and used without further purification. Cumene, p-cymene, 4-fluoroisopropylbenzene, 4-chloroisopropylbenzene, 4-bromoisopropylbenzene, 4-iodoisopropylbenzene, indan and diphenylmethane were purchased from Adamas-beta® and Aladdin®. Chloro(1,5-cyclooctadiene) rhodium(I)dimer ( $[\text{Rh}(\text{cod})\text{Cl}]_2$ ), Rhodium (III) chloride trihydrate ( $\text{RhCl}_3 \cdot 3\text{H}_2\text{O}$ ), Rhodium(II) acetate dimer ( $\text{Rh}_2(\text{OOCCH}_3)_4$ ), Iridium (III) chloride trihydrate ( $\text{IrCl}_3 \cdot 3\text{H}_2\text{O}$ ) and Palladium acetylacetonate ( $\text{Pd}(\text{acac})_2$ ) were purchased from Alfa®. Titanium carbide (TiC, 50 nm), silicon carbide (SiC, 50 nm), vanadium carbide (VC, 50 nm), chromium carbide (CrC, 50 nm), anhydrous Chromium chloride ( $\text{CrCl}_2$ ), anhydrous manganese chloride ( $\text{MnCl}_2$ ), Manganese(II) acetate tetrahydrate ( $\text{Mn}(\text{OAc})_2 \cdot 4\text{H}_2\text{O}$ ), ferrous chloride anhydrous ( $\text{FeCl}_2$ ), cobalt chloride ( $\text{CoCl}_2$ ), Nickel chloride ( $\text{NiCl}_2$ ) anhydrous copper chloride ( $\text{CuCl}_2$ ), zinc chloride ( $\text{ZnCl}_2$ ), iron trifluoromethanesulfonate ( $\text{Fe}(\text{OTf})_3$ ), copper trifluoromethanesulfonate ( $\text{Cu}(\text{OTf})_2$ ), hafnium trifluoromethanesulfonate ( $\text{Hf}(\text{OTf})_4$ ), zinc oxide ( $\text{ZnO}$ ), titanium dioxide ( $\text{TiO}_2$ ), cerium oxide ( $\text{CeO}_2$ ), silicon dioxide ( $\text{SiO}_2$ ), aluminum oxide ( $\text{Al}_2\text{O}_3$ ), magnesium oxide ( $\text{MgO}$ ) and zirconia ( $\text{ZrO}_2$ ) were purchased from Macklin Chemical Reagent Corp. (China). Sodium borohydride ( $\text{NaBH}_4$ ), Methanol (AR, 99.7%), tetrahydrofuran (THF, AR, 99.5%) and acetonitrile (MeCN, AR, 99.5%) were purchased from Sinopharm Chemical. Column chromatography on silica gel (300-400 mesh) was carried out using technical grade 60~90 °C petroleum ether (PE, distilled prior to use) and analytical grade EtOAc (without further purification).

## 2. Characterization

$^1\text{H}$ ,  $^{13}\text{C}$  and  $^{19}\text{F}$  nuclear magnetic resonance spectra were recorded on 400 MHz (Bruker Avance III HD) or 500 MHz (Bruker Avance AV) spectrometer. Chemical shifts were reported in ppm.  $^1\text{H}$  NMR spectra were referenced to  $\text{CDCl}_3$  (7.26 ppm),  $^{13}\text{C}$  NMR spectra was referenced to  $\text{CDCl}_3$  (77.2 ppm). Peak multiplicities were designated by the following abbreviations: s, singlet; d, doublet; t, triplet; m, multiplet; brs, broad singlet and  $J$ , coupling constant in Hz. Coupling constants ( $J$  values) were calculated directly from the spectra. The transmission electron microscopy (TEM, Model JEM-2100F, JEOL) and scanning transmission electron microscopy (STEM, JEM-ARM200F, JEOL) equipped with energy dispersive spectrum (EDS-mapping). X-ray diffraction (XRD) measurements were conducted with a scanning step of  $0.1^\circ/\text{s}$  in the  $2\theta$  range of  $10\text{--}80^\circ$  (D/MAX2200pc). X-ray photon electron spectroscopy (XPS) measurements were performed on an ESCALABMK II X-ray photon electron spectrometer using Mg as the exciting source. The content of Mn and Rh in catalyst were measured by inductively coupled plasma–mass spectrometry (ICP-AES) on an Optima-7000DV system. X-ray absorption near edge structure (XANES) and extended X-ray absorption fine structure (EXAFS) measurements were recorded in fluorescence mode at beamline BL11B station at Shanghai Synchrotron Radiation Facility (SSRF). Data was analyzed using the Athena and Artemis software in the Demeter package.

## 3. Computational method

All spin-polarized density functional theory (DFT) method were performed using the Vienna ab initio simulation package (VASP) code with the projector augmented wave (PAW) method.<sup>S1</sup> The generalized gradient approximation (GGA) combined with Perdew-Burke-Ernzerhof (PBE) functional was employed to describe the exchange-correlation term.<sup>S2</sup> The projector augmented wave (PAW) pseudo-potentials were used to describe ionic cores.<sup>S3</sup> A vacuum space of 15 Å along the z-axis was added to avoid the interactions between periodic slabs. The cutoff energy for the plane-wave basis was

set to 450 eV. The Van der Waals (vdW) interactions was described by using the empirical correction in Grimme's scheme (DFT-D3) in all calculations.<sup>4</sup> The convergence tolerances for energy and force were set to  $10^{-5}$  eV and 0.05 eV/Å, respectively. The Gibbs free energy change ( $\Delta G$ ) for each elemental step was defined as flows.

$$\Delta G = \Delta E_{DFT} + \Delta E_{ZPE} - T\Delta S$$

In this equation,  $\Delta E_{DFT}$  is denotes the electronic energy change directly obtained from DFT calculations,  $\Delta E_{ZPE}$  and  $\Delta S$  are the zero-point energy correction and entropy change obtained from frequency calculations at 298.15 K.

## 4. Supplementary experimental section

### Preparation of oxygen-modified carbon-based support

Take O-TiC as an example. The commercial nano TiC support powder (500 mg) was placed in a 250 mL round bottom flask, sonicated and dispersed into 5 M sodium hydroxide solution (NaOH, 150 mL), kept sonicated for 30 min, stirred overnight (usually 12 h) at 70 °C, 1000 rpm, the mixture was cooled to room temperature, filtered, the solid was washed several times with methanol and DI water, and dried under vacuum at 60 °C for 10 h. The black O-TiC sample was obtained. (O-VC, O-CrC and O-SiC were synthesized in the same way)

### Preparation of single-atom catalyst ( $M_1@MO_x$ , $M_1@TiN$ and $M_1@O-TiC$ )

100 mg of support was ultrasonically dispersed into 50 mL of DI water (as for  $M_1@MO_x$ ) or mixed solution (50 mL, DI water: MeOH = 1:1), and then the prepared metal salt solution (5 mg/mL) was added dropwise to the oxide support mixture at a rate of 36  $\mu$ L/min (via autosampler), each drop has a volume of 5~10  $\mu$ L. After the dropwise addition, the solution was stirred at 60 °C for 6 h. The solid was filtered (0.2  $\mu$ m organic filter membranes are used here), washed with ethanol and DI water several times, and dried under vacuum at 60 °C for 10 h. After drying, the solid was put into a Schlenk tube (25 mL) and collected the solid. (M = Cr, Mn, Fe, Co, Ni, Cu, Zn)

### Preparation of dual single-atom catalyst

Take  $Mn_1-Rh_1@O-TiC$  as an example. 100 mg of O-TiC was added into a three-port flask (250 mL) containing DI water (90 mL) and methanol (10 mL, DI water: methanol= 9:1) and then dispersed by ultrasonication for 30 min to form a uniform suspension. Then a certain dose of metallic precursor solution ( $MnCl_2$ ,  $RhCl_3 \cdot 3H_2O$ , two metals need to be loaded separately) was dissolved into DI water was added dropwise to the O-TiC mixture at a rate of 36  $\mu$ L/min (via autosampler), each drop has a volume of 5~10  $\mu$ L. After the dropwise addition, the solution was stirred at 60 °C for 6 h. The solid was filtered (0.2  $\mu$ m organic filter membranes are used here), washed with methanol and DI water several times, and dried under vacuum at 60 °C for 10 h.  $Mn_1@O-TiC$  and  $Rh_1@O-TiC$  catalyst were obtained. The dried two samples were then

physical mixed and homogeneously ground through an agate mortar (approximately 30 min). ( $\text{Mn}_1\text{-Pd}_1\text{@O-TiC}$ ,  $\text{Mn}_1\text{-Fe}_1\text{@O-TiC}$ ,  $\text{Mn}_1\text{-Cu}_1\text{@O-TiC}$ ,  $\text{Fe}_1\text{-Rh}_1\text{@O-TiC}$ ,  $\text{Cu}_1\text{-Rh}_1\text{@O-TiC}$ ,  $\text{Mn}_1\text{-Hf}_1\text{@O-TiC}$ ,  $\text{Mn}_1\text{-Rh}_1\text{@TiO}_2$ ,  $\text{Mn}_1\text{-Rh}_1\text{@TiN}$ ,  $\text{Mn}_1\text{-Rh}_1\text{@O-SiC}$ ,  $\text{Mn}_1\text{-Rh}_1\text{@O-VC}$ ,  $\text{Mn}_1\text{-Rh}_1\text{@O-CrC}$ , these catalysts were synthesized in the same way, except that the solvents used to partially dissolve the metal salts are different. Details of the physical mixing ratios of  $\text{Mn}_1\text{@O-TiC}$  and  $\text{Rh}_1\text{@O-TiC}$  are given in **Table S18**.)

#### **Preparation of Nanocluster catalyst (Mn-Rh NC/O-TiC)**

100 mg of O-TiC was added into a three-port flask (250 mL) containing DI water (90 mL) and methanol (10 mL, DI water: methanol = 9:1) and then dispersed by ultrasonication for 30 min to form a uniform suspension. 5 mg of  $\text{Mn(OAc)}_2\cdot 4\text{H}_2\text{O}$  was dissolved in 1 mL of DI water and 5 mg of  $[\text{Rh}_2(\text{OOCCH}_3)_4]$  were dissolved in 1 mL of methanol. Subsequently, the two solutions were added directly to the O-TiC suspension. The mixture solution was then stirred for 2 h at room temperature and then at 60 °C for 6 h. After cooling to room temperature, the solid was thoroughly washed and collected by a filtration method, and then dried in a vacuum oven at 60 °C overnight. Mn-Rh NC/O-TiC catalyst was obtained.

#### **Preparation of Nano particle catalyst (Mn NP/O-TiC and Rh NP/O-TiC)**

100 mg of O-TiC was added into a three-port flask (250 mL) containing DI water (90 mL) and methanol (10 mL, DI water: methanol = 9:1) and then dispersed by ultrasonication for 30 min to form a uniform suspension. 5 mg of  $\text{Mn(OAc)}_2\cdot 4\text{H}_2\text{O}$  was dissolved in 1 mL of DI water was dissolved in 1 mL of methanol. Subsequently, the two solutions were added directly to the O-TiC suspension. Subsequently, an appropriate amount of aqueous sodium borohydride solution was added, and the mixture was stirred for an additional 2 hours at room temperature and then at 60 °C for 6 h. After cooling to room temperature, the solid was thoroughly washed and collected by a filtration method, and then dried in a vacuum oven at 60 °C overnight. Mn NP/O-TiC catalyst was obtained. Rh NP/O-TiC was synthesized in the same way except that the metal salt was changed to  $[\text{Rh}_2(\text{OOCCH}_3)_4]$ .

Conversion and selectivity for substrates and their products were calculated as the following equations

$$\text{Conversion (\%)} = N_r / N_i$$

where  $N_r$  indicate moles of reacted substrates,  $N_i$  indicate moles of initial substrates

Selectivity for corresponding product (%) = (corresponding product/total products) × 100%

Calculation of turnover numbers (TON) with the following equation

$$\text{TON} = N_s / N_c$$

where  $N_s$  indicate moles of reacted substrates,  $N_c$  indicate moles of reacted metal catalyst (metal content based on ICP test).  $N_c$  is  $2.37 \times 10^{-3}$  mmol. Under standard conditions, the yield of the target product acetophenone (2a) obtained from the reaction of 2.9 mmol of substrate was 94%,  $N_s$  is 2.731 mmol. TON is 1152.

#### **General procedure for C-H bond oxidation**

Catalytic C-H oxidation reactions of various substrates, including cumene, p-cymene, 4-fluoroisopropylbenzene, 4-chloroisopropylbenzene, 4-bromoisopropylbenzene, 4-iodoisopropylbenzene, indan and diphenylmethane, were carried out in 10 mL Schlenk tube. Take oxygenation of cumene on  $\text{Mn}_1\text{-Rh}_1\text{@O-TiC}$  as example. The  $\text{Mn}_1\text{-Rh}_1\text{@O-TiC}$  (40 mg, 0.08 mol%), cumene (0.4 mL, 2.9 mmol) was added sequentially to a clean Schlenk tube (10 mL), a magnetic stirrer (1 cm in diameter) was added to the tube, then an oxygen balloon was placed over the branch port and the gas was pumped three times. Then ultrasound dispersion for 20 minutes and stirred at 120 °C, 400 rpm for 12-18 h. After it cooled to room temperature, the conversion and the selectivity were determined by gas chromatograph–mass spectrometer (Agilent Intuvo 9000 GC-MS). Then, the resulting mixture was transferred to a silica gel column. The tube was washed with EtOAc (2 mL × 3) and then transferred to a silica gel column. Then through flash chromatography on silica gel (PE / EtOAc: 50/1-20/1), the mixture was purified to afford a pure product.

#### **General procedure for scale-up cumene oxidation**

The  $\text{Mn}_1\text{-Rh}_1\text{@O-TiC}$  (800 mg, 0.08 mol%), cumene (8 mL, 58 mmol) was added sequentially to a clean Schlenk flask (50 mL), then an oxygen balloon was placed over



the branch port and the gas was pumped three times. Then ultrasound dispersion for 20 minutes and stirred at 120 °C, 400 rpm for 74 h. After it cooled to room temperature, the conversion of CM and the selectivity of AP were determined by gas chromatograph-mass spectrometer (Agilent Intuvo 9000 GC-MS). Then, the resulting mixture was transferred to a silica gel column. The tube was washed with EtOAc (2 mL × 3) and then transferred to a silica gel column. Then through flash chromatography on silica gel (PE / EtOAc: 30/1), the mixture was purified to afford a pure product (AP).

### Recycling studies

To study the recyclability of Mn<sub>1</sub>-Rh<sub>1</sub>@O-TiC, the acetophenone was conducted under the same conditions as described above general procedure. After reaction, the catalyst was separated through centrifugation and the catalyst was washed with DI water, methanol, and ethyl acetate successively. And then dried in a vacuum oven at 60 °C overnight and reused in a next run.

### Hot filtration experiment

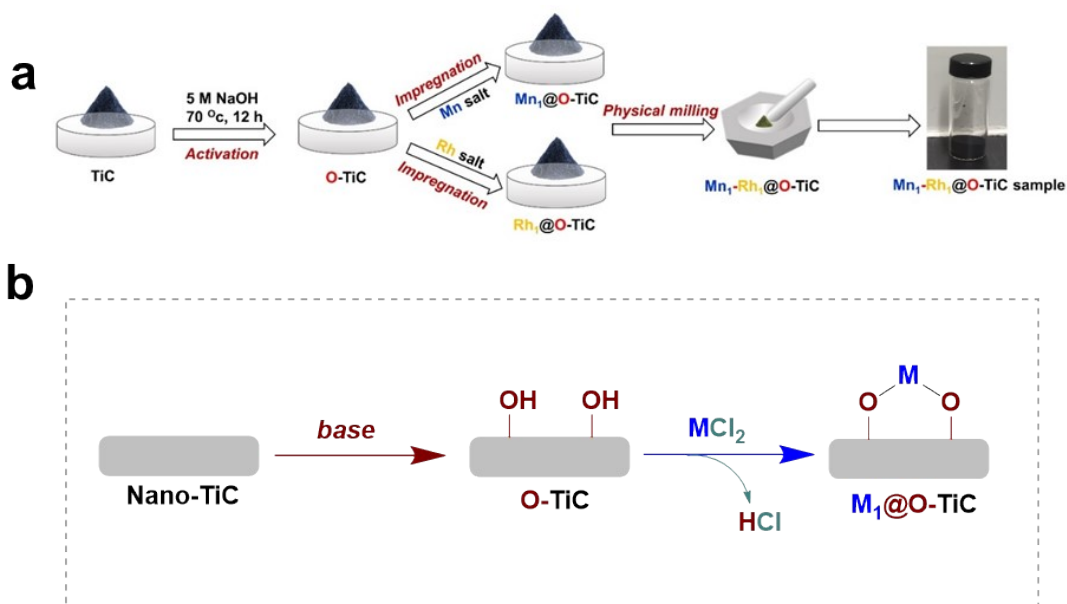
We tested the kinetics of the reaction by thermal filtration tests (**Figure S15**). After 5 h of catalysis at 120 °C, we removed the Mn<sub>1</sub>-Rh<sub>1</sub>@O-TiC catalyst. The conversion of cumene did not change significantly after removing the Mn<sub>1</sub>-Rh<sub>1</sub>@O-TiC catalyst. This indicates that the activity of the reaction was catalyzed by the Mn<sub>1</sub>-Rh<sub>1</sub>@O-TiC catalyst, and we did not find any metal leaching by ICP-AES test (**Table S20**).

### Control experiments

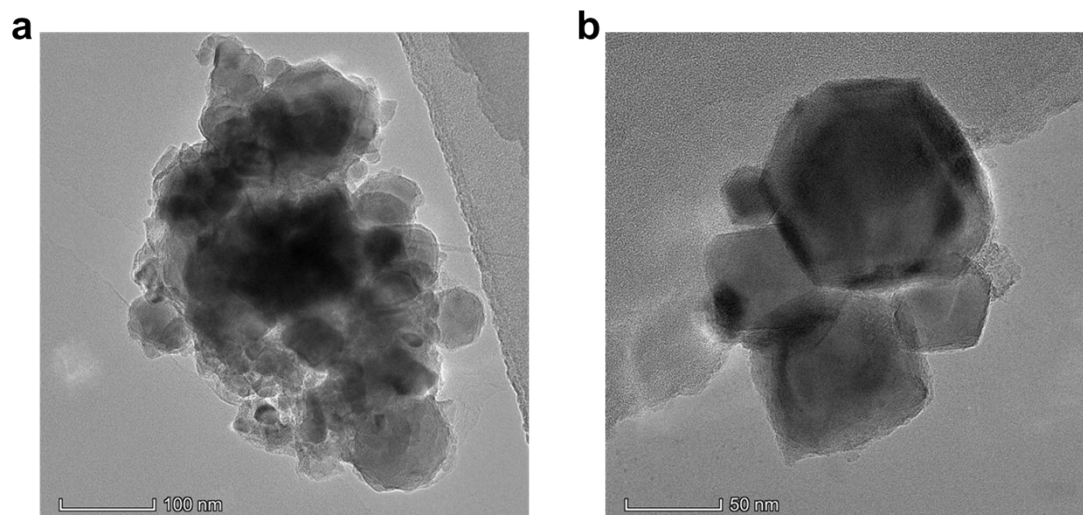
Dehydration of BP: The Rh<sub>1</sub>@O-TiC (40 mg) or Mn<sub>1</sub>@O-TiC (40 mg), BP (dimethyl phenyl methanol, 0.41 mL, 2.9 mmol) was added sequentially to a clean Schlenk tube (10 mL), a magnetic stirrer (1 cm in diameter) was added to the tube, then ultrasound dispersion for 20 minutes and stirred at 120 °C, 400 rpm for 24 h. After the resulting mixture was cooled to room temperature quickly, the conversion of BP and selectivity of AMS were calculated by GC-MS (**Table. S15**).

Oxidative cleavage of AMS: The Mn<sub>1</sub>@O-TiC (40 mg) or Rh<sub>1</sub>@O-TiC (40 mg), AMS ( $\alpha$ -methyl styrene, 0.38 mL, 2.9 mmol) was added sequentially to a clean Schlenk tube (10 mL), a magnetic stirrer (1 cm in diameter) was added to the tube, then an oxygen

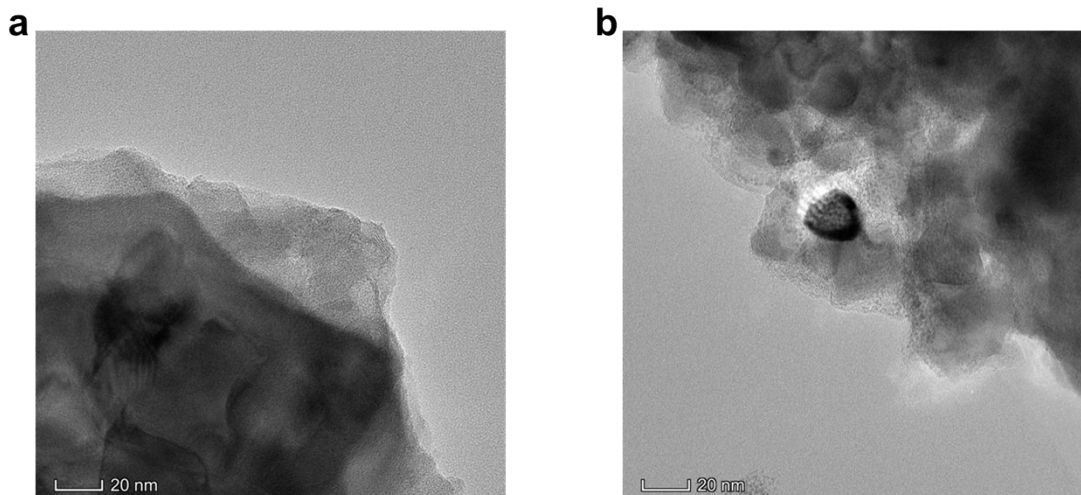
balloon was placed over the branch port and the gas was pumped three times. Then ultrasound dispersion for 20 minutes and stirred at 120 °C, 400 rpm for 24 h. After the resulting mixture was cooled to room temperature quickly, the conversion of AMS and selectivity of AP were calculated by GC-MS (**Table. S16**).



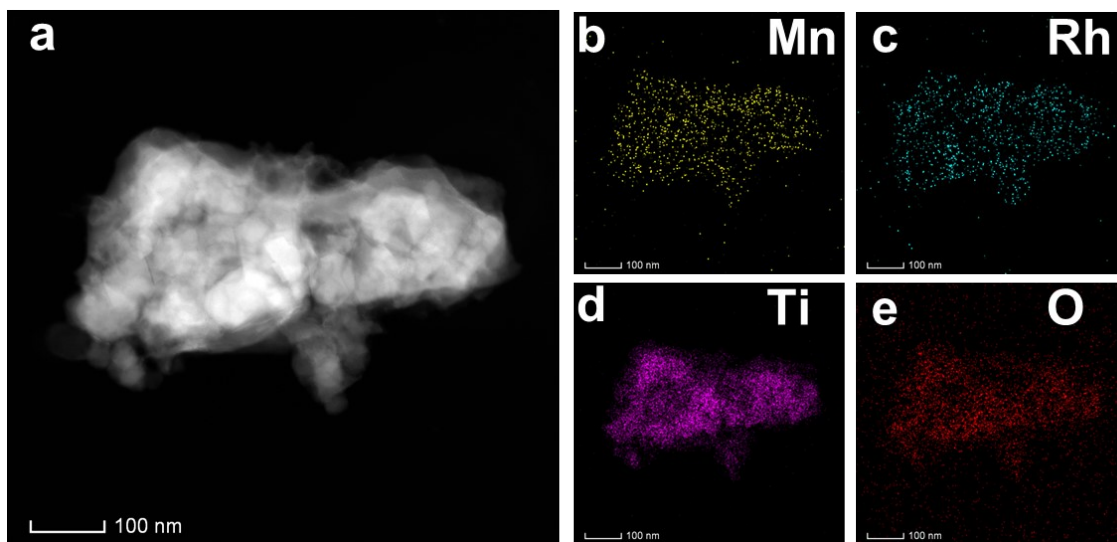
**Figure S1.** Schematic diagram of Mn<sub>1</sub>-Rh<sub>1</sub>@O-TiC dual single atom catalyst.



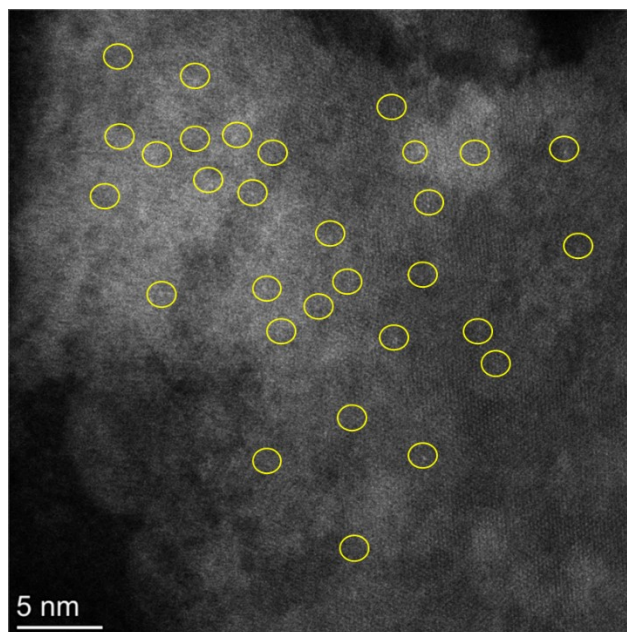
**Figure S2.** The TEM images of Mn<sub>1</sub>-Rh<sub>1</sub>@O-TiC-fresh (a), Mn<sub>1</sub>-Rh<sub>1</sub>@O-TiC-used (b).



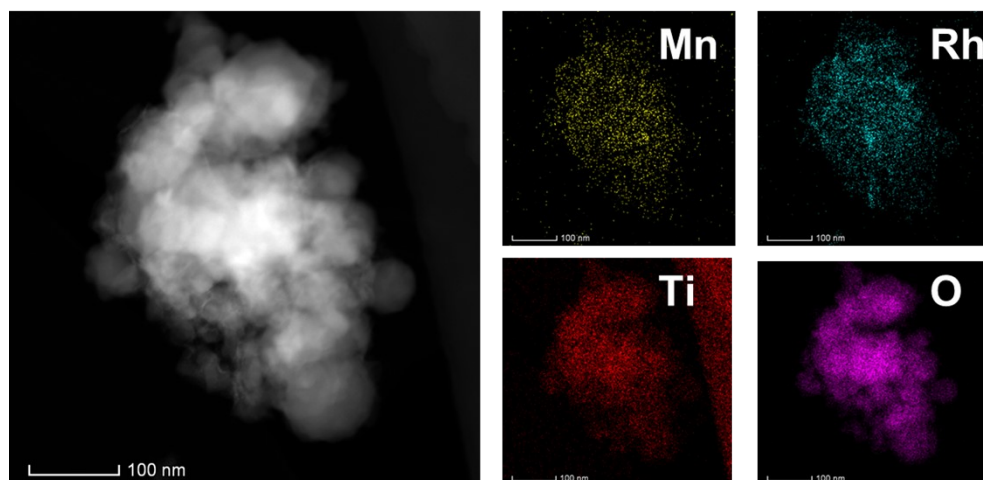
**Figure S3.** The HR-TEM images of  $\text{Mn}_1\text{-Rh}_1\text{@O-TiC}$ -fresh (a),  $\text{Mn}_1\text{-Rh}_1\text{@O-TiC}$ -used (b).



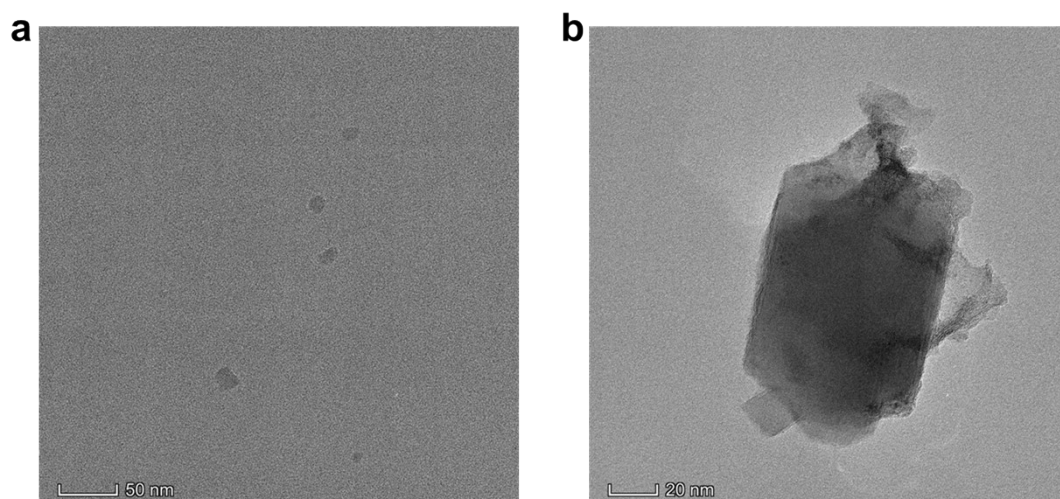
**Figure S4.** Elemental mapping images of Mn<sub>1</sub>-Rh<sub>1</sub>@O-TiC-fresh (gold: Mn, cyne: Rh, purple: Ti, red: O).



**Figure S5.** Spherical aberration-corrected HAADF-STEM image of  $\text{Mn}_1\text{-Rh}_1\text{@O-TiC-used}$ .

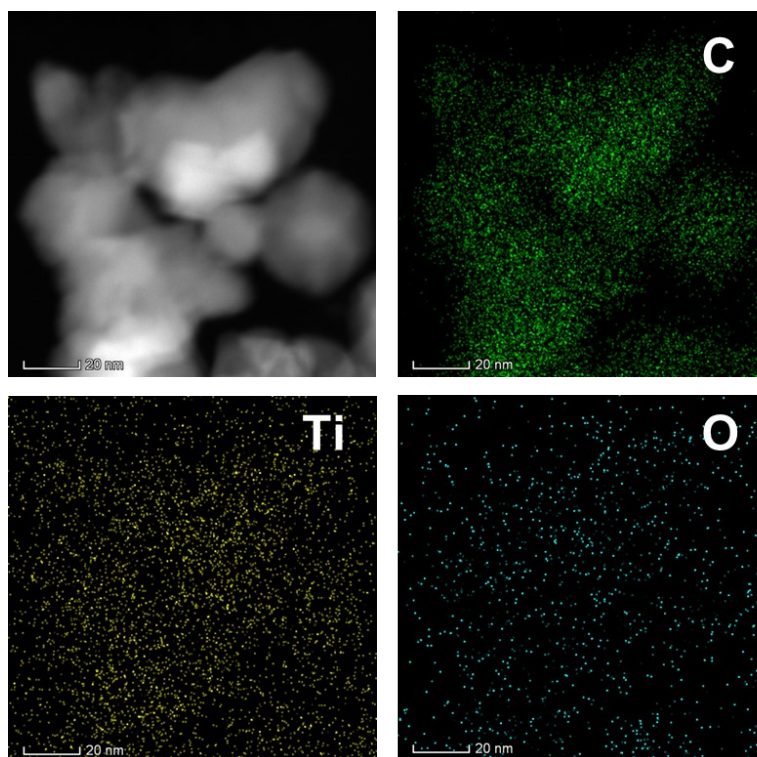


**Figure S6.** Elemental mapping images of  $\text{Mn}_1\text{-Rh}_1\text{@O-TiC-used}$  (gold: Mn, cyne: Rh, Red: Ti, purple: O).

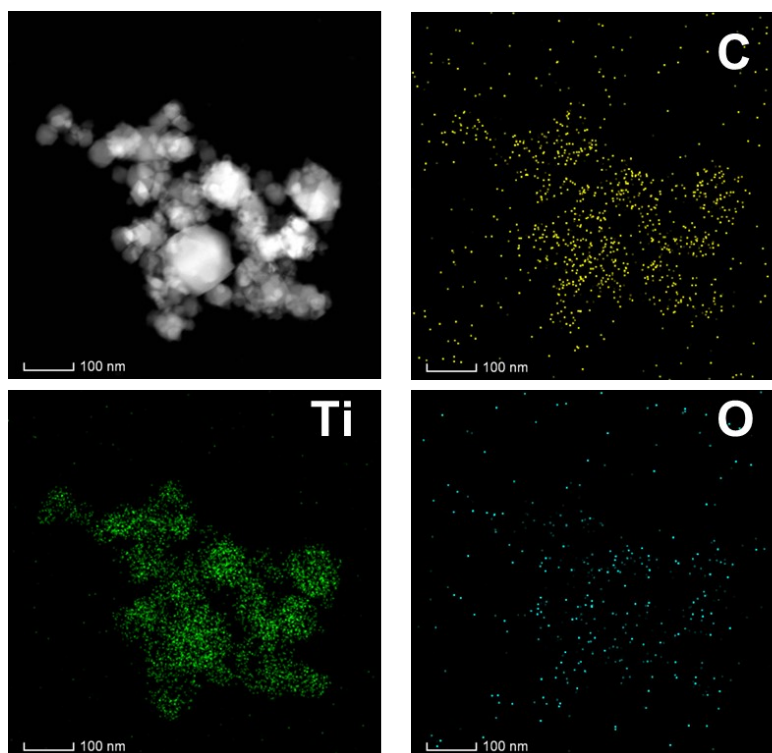


**Figure S7.** The HR-TEM images of TiC (a), O-TiC (b).

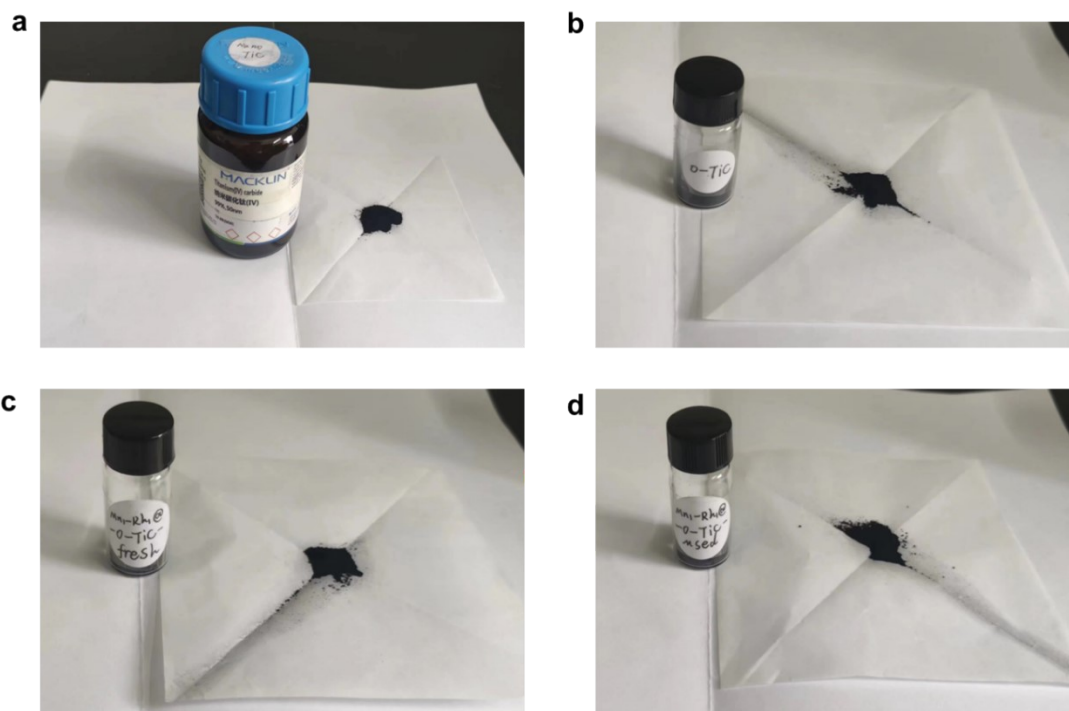




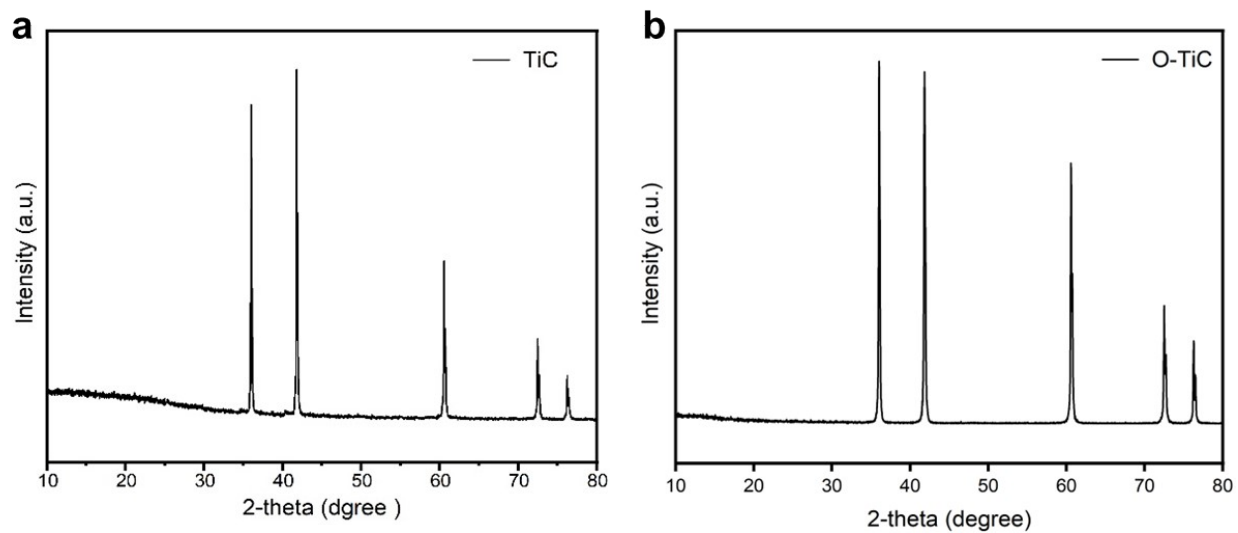
**Figure S8.** Elemental mapping images of O-TiC (green: C, gold: Ti, cyne: O).



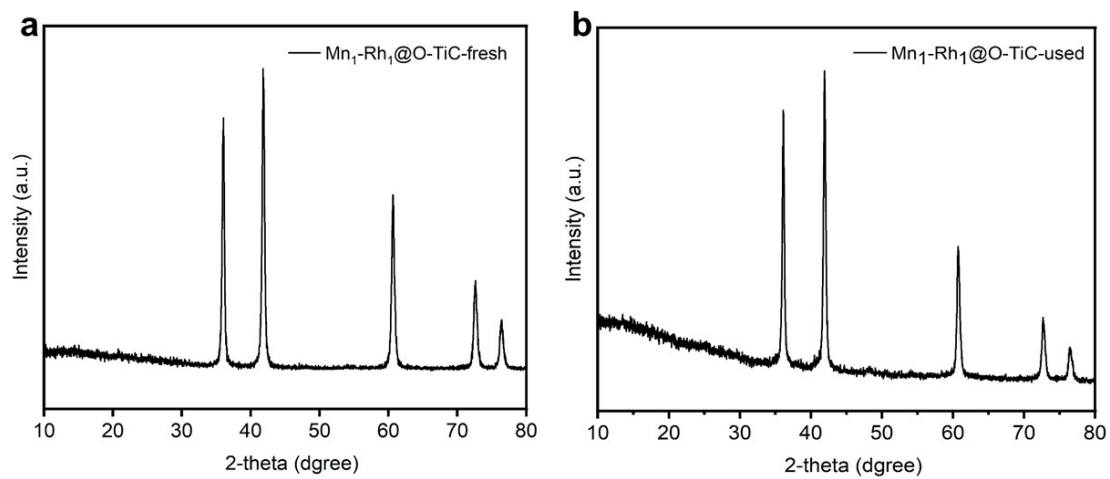
**Figure S9.** Elemental mapping images of TiC (gold: C, green: Ti, cyne: O).



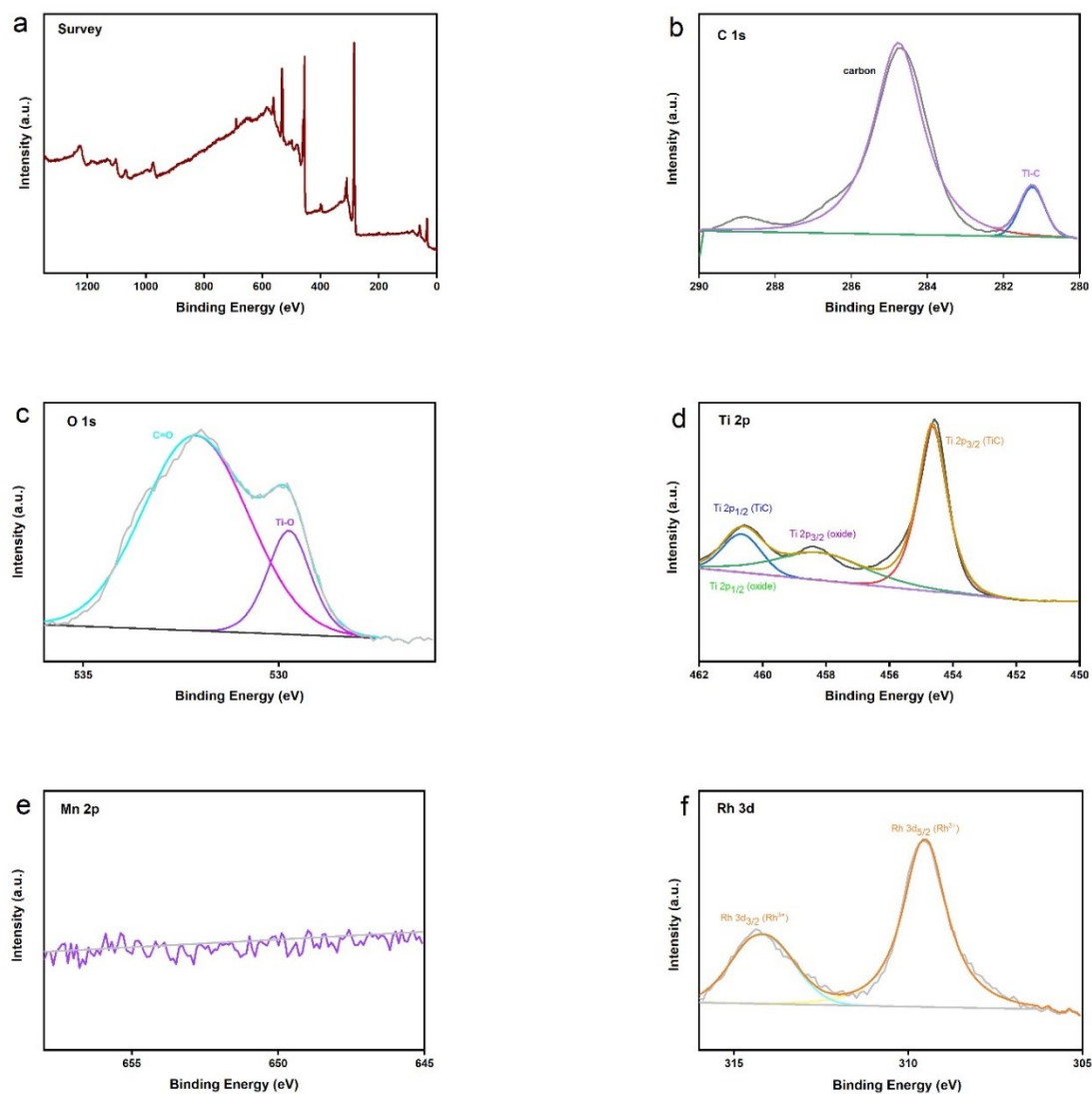
**Figure S10.** The images of commercial nano TiC (a), oxygen-modified carbon-based support O-TiC (b),  $\text{Mn}_1\text{-Rh}_1\text{@O-TiC-fresh}$  (c) and  $\text{Mn}_1\text{-Rh}_1\text{@O-TiC-used}$  (d).



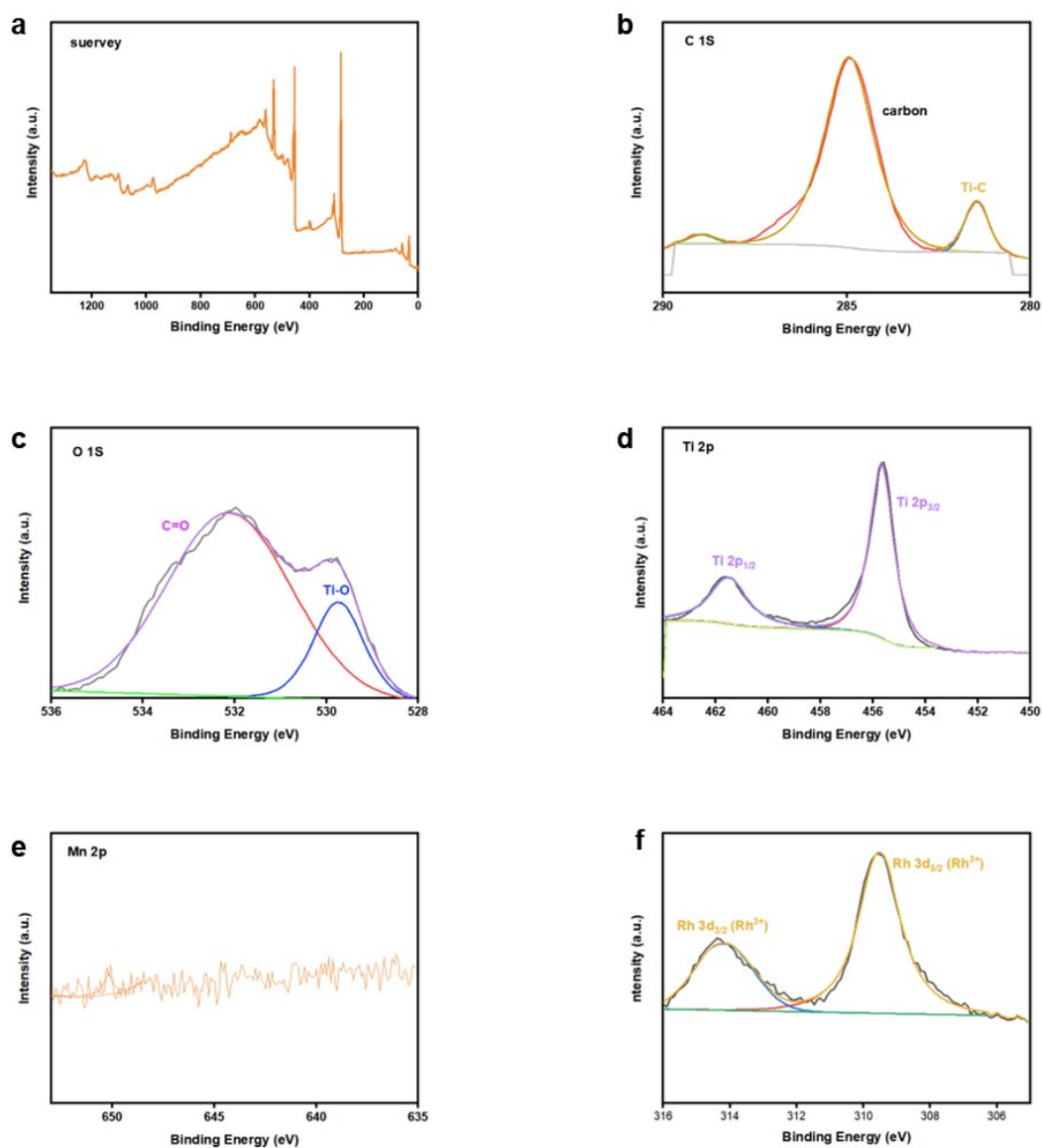
**Figure S11.** The XRD of the TiC (a) and O-TiC (b).



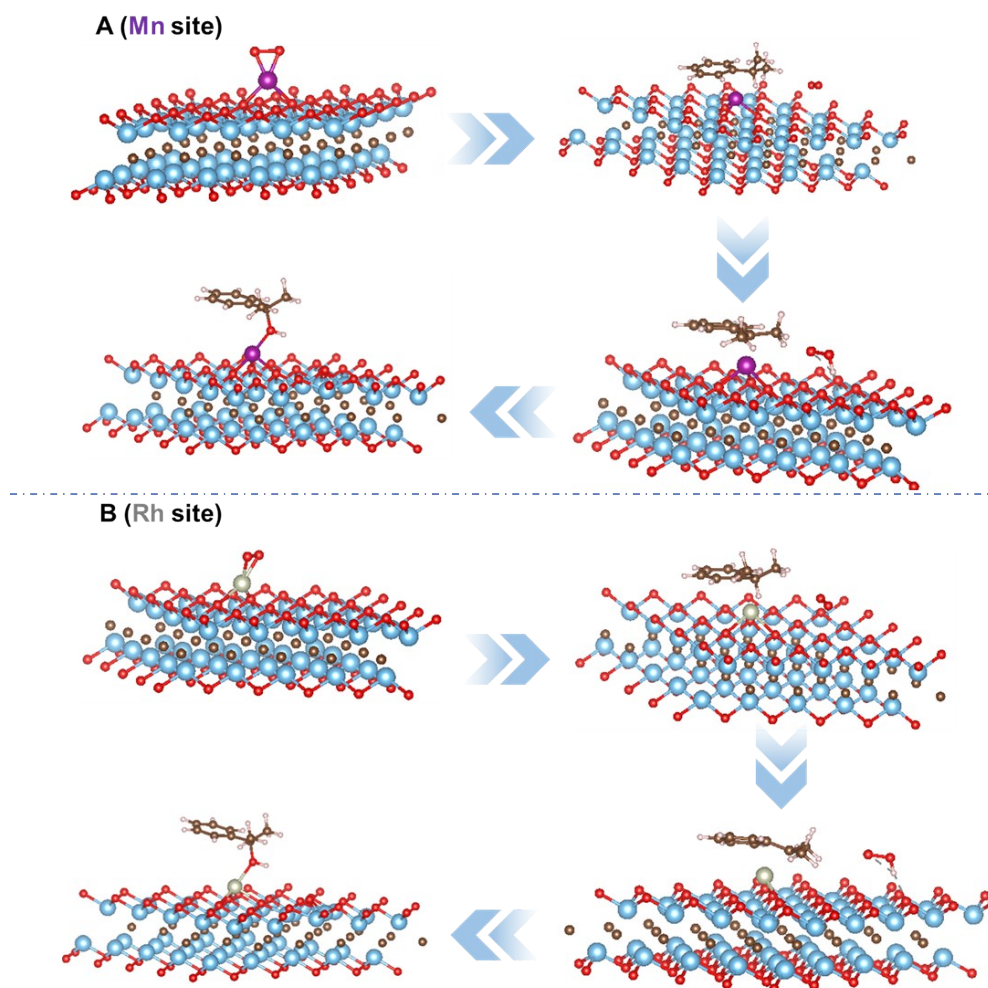
**Figure S12.** The XRD of the  $\text{Mn}_1\text{-Rh}_1\text{@O-TiC-fresh}$  (a) and  $\text{Mn}_1\text{-Rh}_1\text{@O-TiC-used}$  (b).



**Figure S13.** The XPS of the Mn<sub>1</sub>-Rh<sub>1</sub>@O-TiC-fresh, including the orbitals of (a) the survey, (b) C 1s, (c) O 1s and (d) Ti 2p, (e) Mn 2p and (f) Rh 3d.



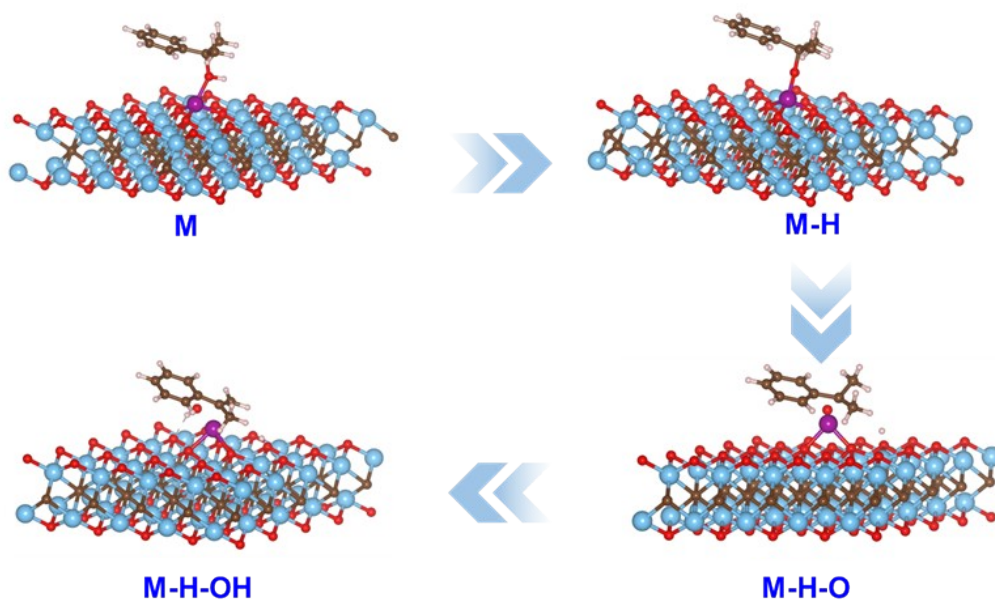
**Figure S14.** The XPS of the  $\text{Mn}_1\text{-Rh}_1\text{@O-TiC-used}$ , including the orbitals of (a) the survey, (b) C 1s, (c) O 1s and (d) Ti 2p, (e) Mn 2p and (f) Rh 3d.



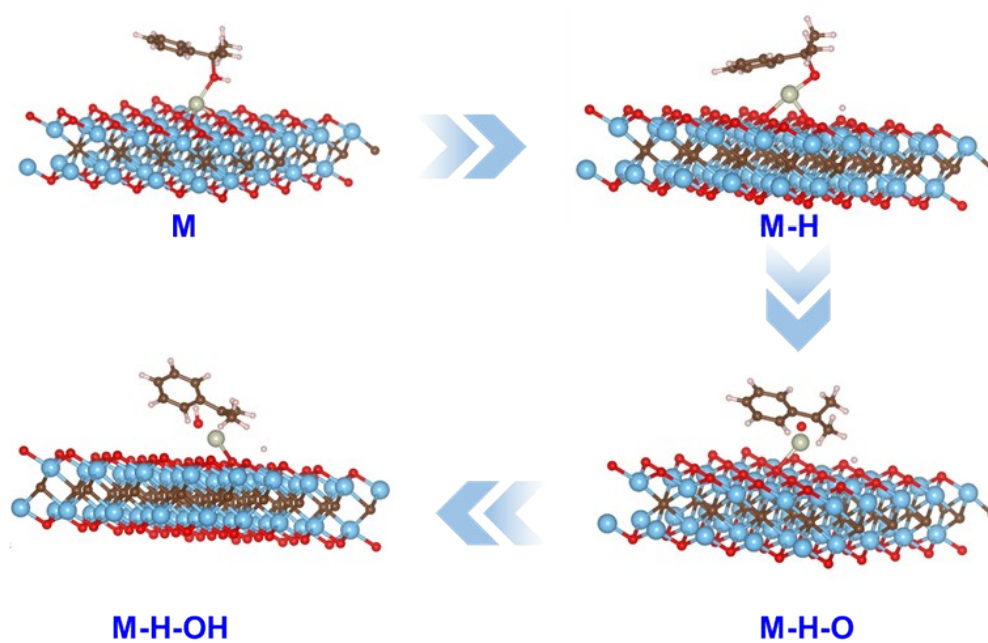
**Figure S15.** The optimized structure of Mn site and Rh site in the conversion of CM to BP process. (brown: C, white: H, red: O, blue: Ti purple: Mn, gray: Rh)



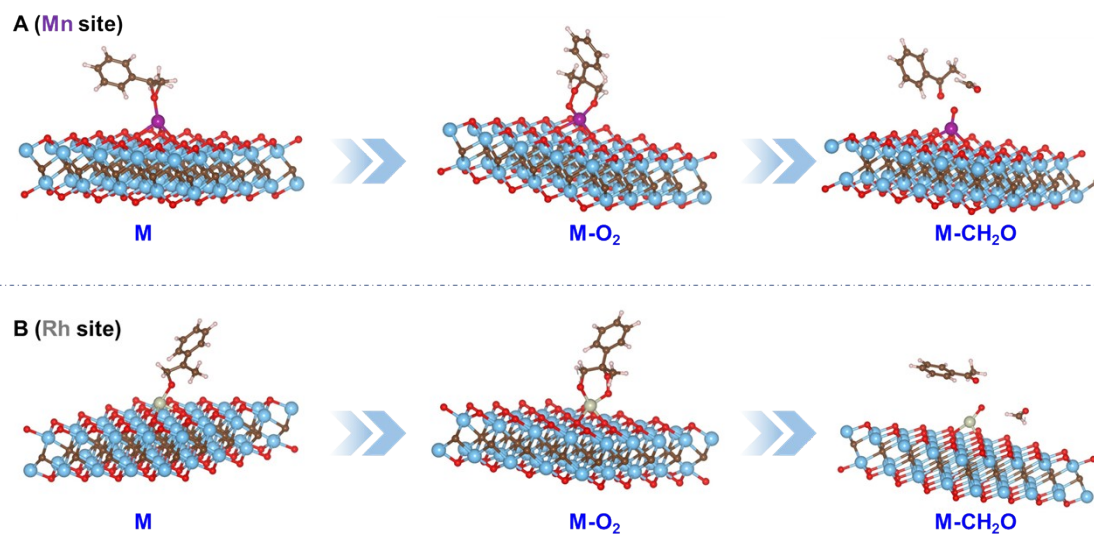
**A (Mn site)**



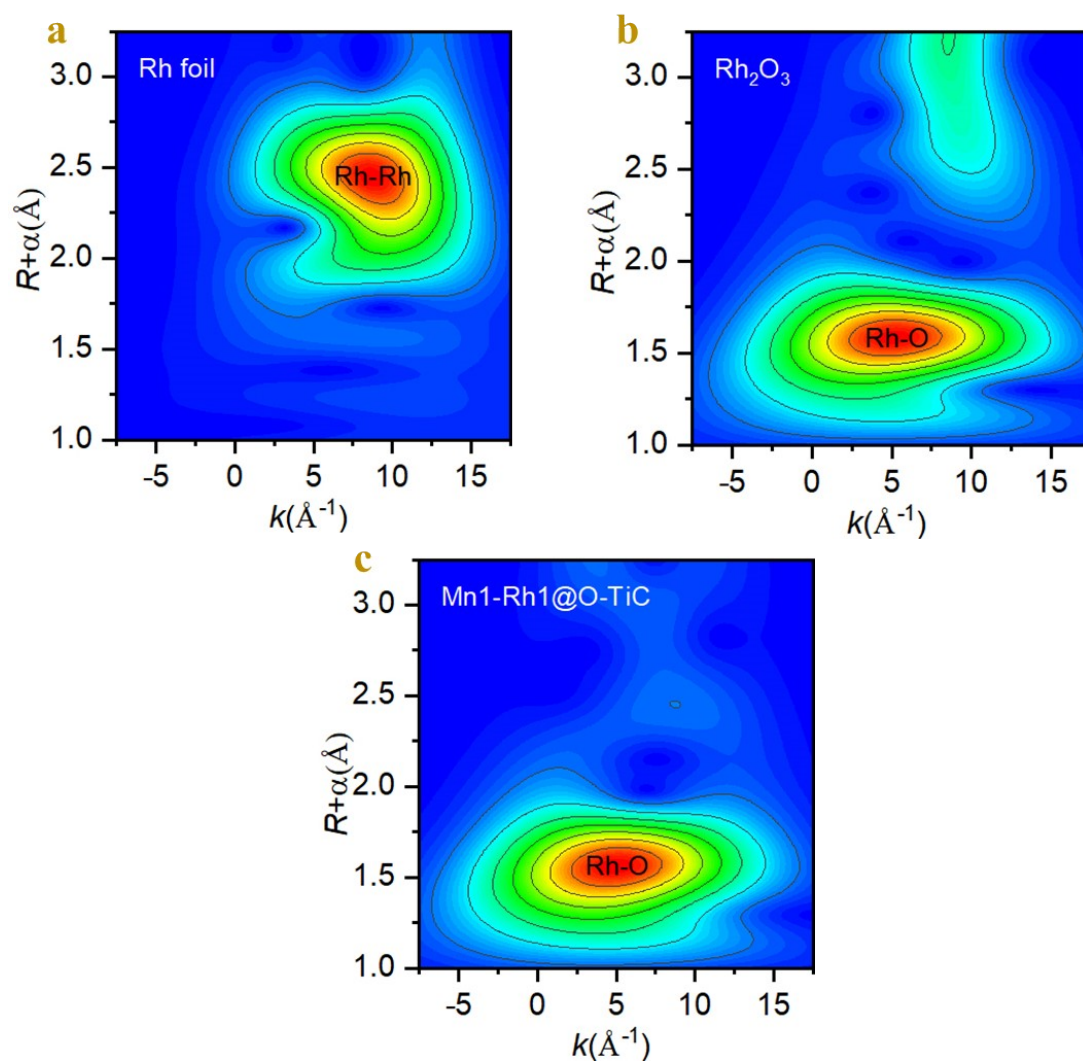
**B (Rh site)**



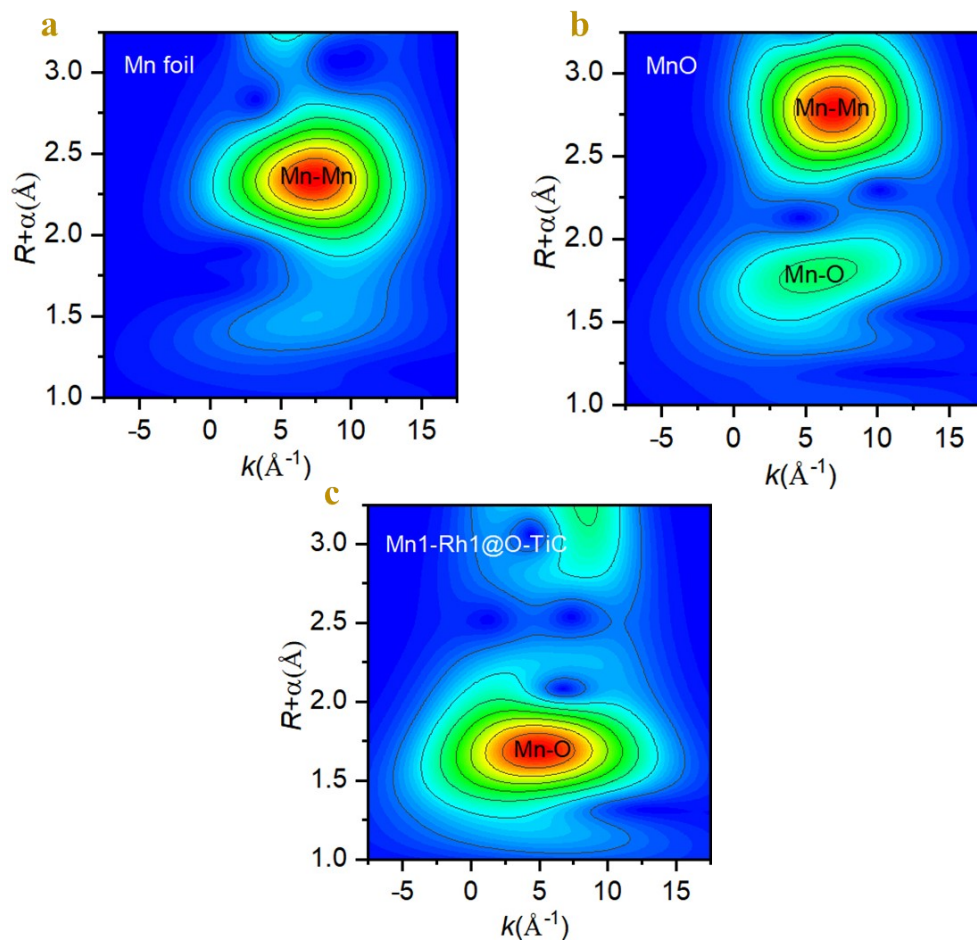
**Figure S16.** The optimized structure of Mn site and Rh site in the dimethyl phenyl methanol dehydration reaction.(brown: C, white: H, red: O, blue: Ti purple: Mn, gray: Rh)



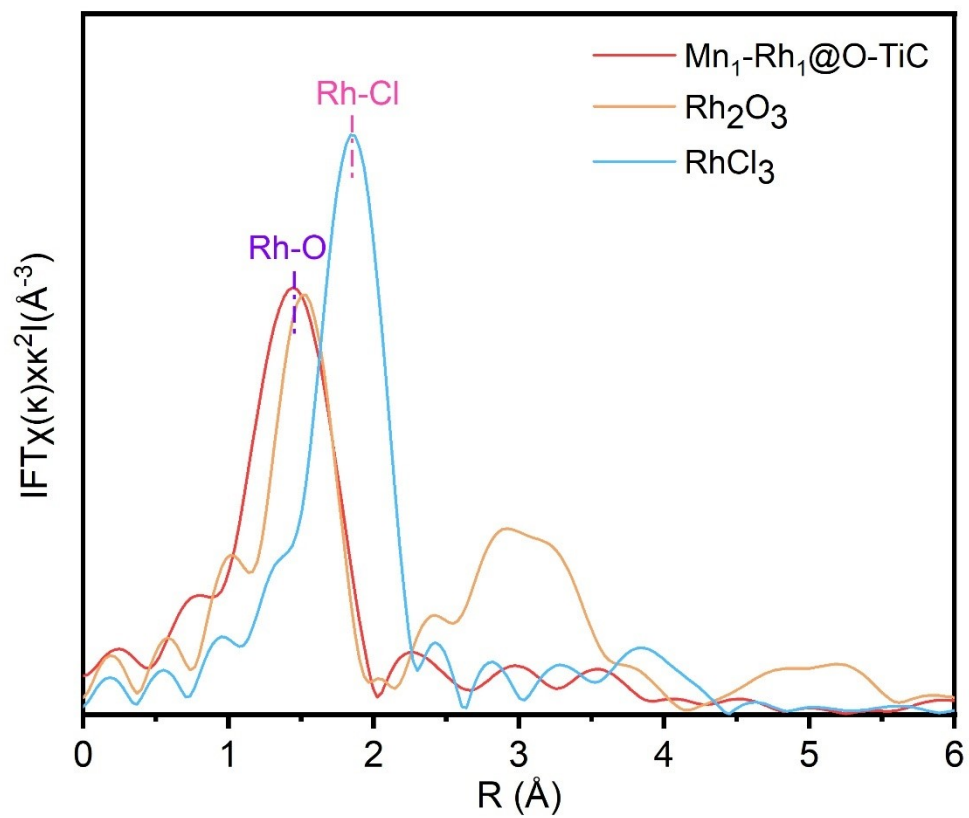
**Figure S17.** The optimized structure of Mn site and Rh site in the  $\alpha$ -methyl styrene oxidative cracking reaction.(brown: C, white: H, red: O, blue: Ti purple: Mn, gray: Rh)



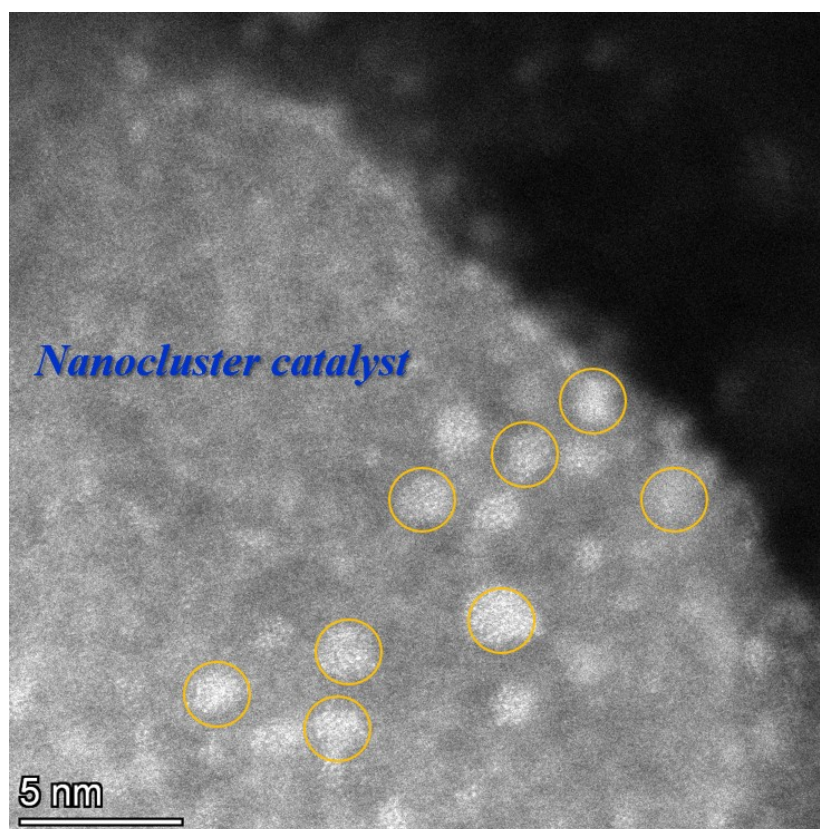
**Figure S18.** Wavelet transforms (WT) of the results of Rh foil (a),  $\text{Rh}_2\text{O}_3$  (b) and  $\text{Mn}_1\text{-Rh}_1\text{@O-TiC}$ .



**Figure S19.** Wavelet transforms (WT) of the results of Mn foil (a), MnO (b) and Mn<sub>1</sub>-Rh<sub>1</sub>@O-TiC.

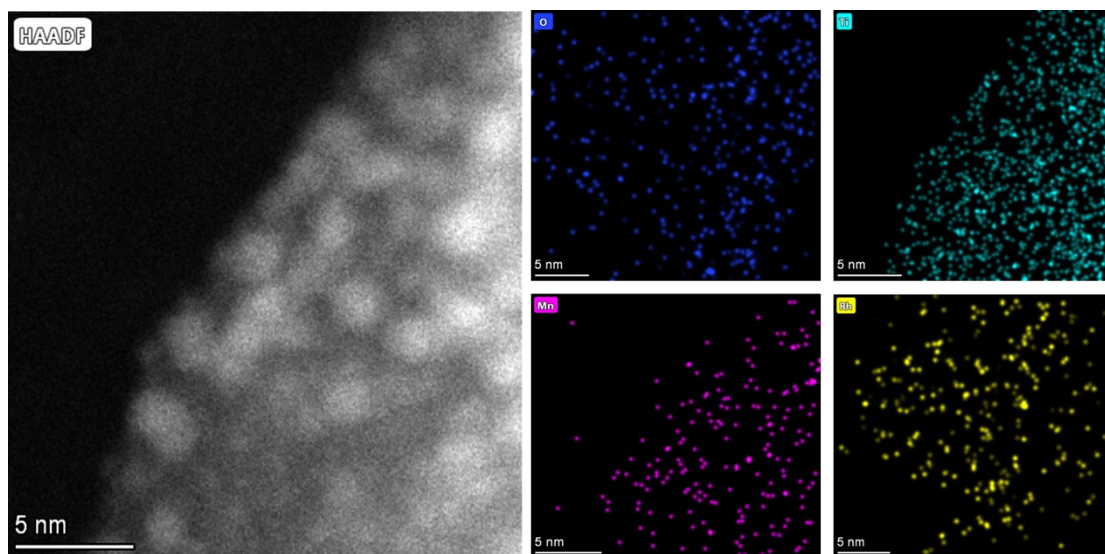


**Figure S20.** FT-EXAFS and the fitting of the  $\text{RhCl}_3$ ,  $\text{Rh}_2\text{O}_3$ ,  $\text{Mn}_1\text{-Rh}_1\text{@O-TiC}$ .

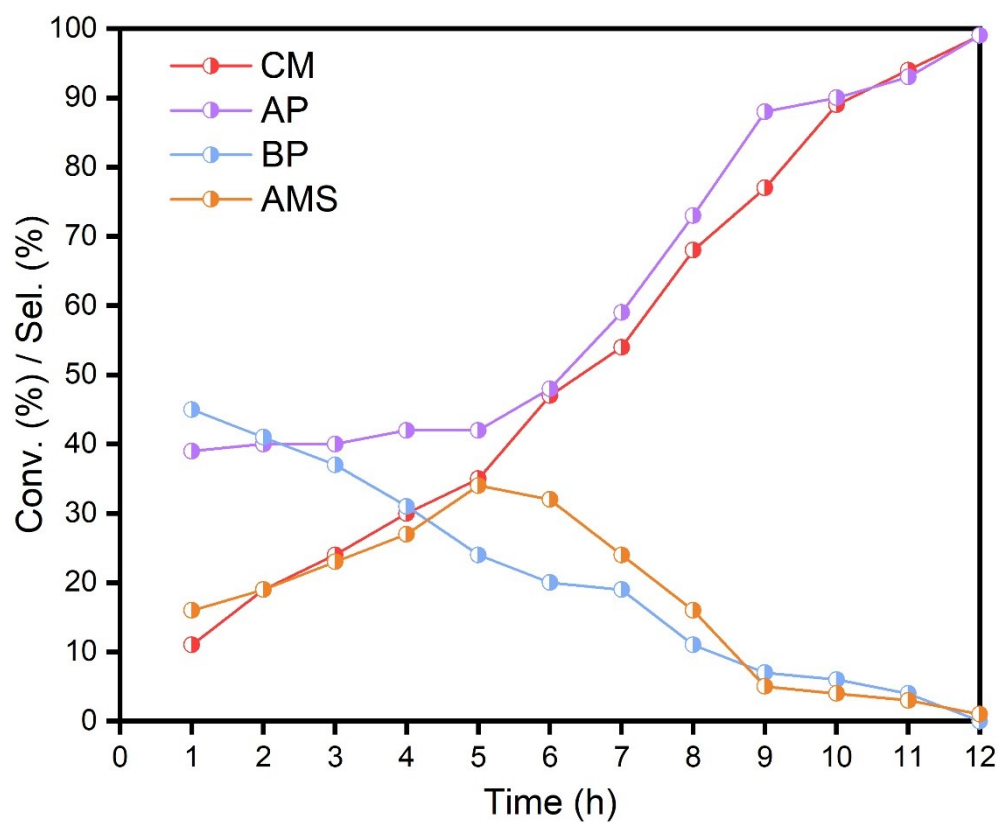


**Figure S21** AC-HAADF-STEM of Mn-Rh NC/O-TiC.





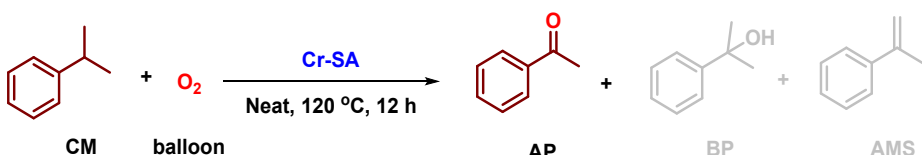
**Figure S22** HAADF-STEM images and corresponding elemental EDXS mapping of Mn-Rh NC/O-TiC (blue: O, cyan: Ti, purple: Mn, gold: Rh)



**Figure S23.** Kinetic curve diagram (CM : cumene, BP: dimethyl phenyl methanol, AMS:  $\alpha$ -methyl styrene, AP: acetophenone)

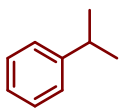

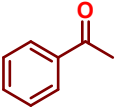
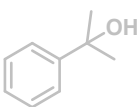
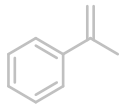


**Table S1.** Screening of Cr single-atom catalyst <sup>ab</sup>

 <div>CM + O<sub>2</sub> <math>\xrightarrow[\text{Neat, 120 } ^\circ\text{C, 12 h}]{\text{Cr-SA}}</math> AP + BP + AMS</div>		
Entry	Catalyst	Conv. (%) <sup>b</sup>
1	Cr <sub>1</sub> @CeO <sub>2</sub>	7.3
2	Cr <sub>1</sub> @ZnO	7.2
3	Cr <sub>1</sub> @MgO	15
4	Cr <sub>1</sub> @SiO <sub>2</sub>	-
5	Cr <sub>1</sub> @Al <sub>2</sub> O <sub>3</sub>	-
6	Cr <sub>1</sub> @ZrO <sub>2</sub>	-

<sup>a</sup> Cr-SA (40 mg), CM (2.9 mmol, 0.4 mL), 400 rpm; <sup>b</sup> Conversion was determined by GC-MS analysis with internal standard (*n*-dodecane); Conv. = Conversion; “-” means no reaction.

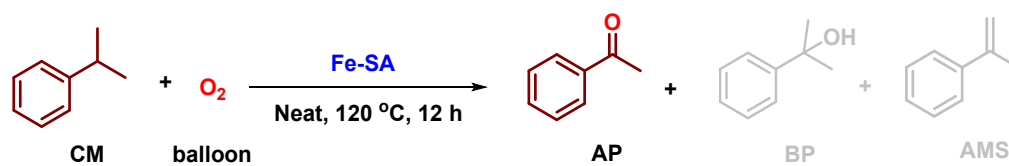
**Table S2.** Screening of Mn single-atom catalyst <sup>ab</sup>

	+		$\xrightarrow[\text{Neat, 120 } ^\circ\text{C, 12 h}]{\text{Mn-SA}}$		+		+	
CM		balloon		AP		BP		AMS

Entry	Catalyst	Conv. (%) <sup>b</sup>
1	Mn <sub>1</sub> @CeO <sub>2</sub>	90
2	Mn <sub>1</sub> @ZnO	88
3	Mn <sub>1</sub> @MgO	42
4	Mn <sub>1</sub> @SiO <sub>2</sub>	-
5	Mn <sub>1</sub> @Al <sub>2</sub> O <sub>3</sub>	26
6	Mn <sub>1</sub> @ZrO <sub>2</sub>	6

<sup>a</sup> Mn-SA (40 mg), CM (2.9 mmol, 0.4 mL), 400 rpm; <sup>b</sup> Conversion was determined by GC-MS analysis with internal standard (*n*-dodecane); “-” means no reaction.

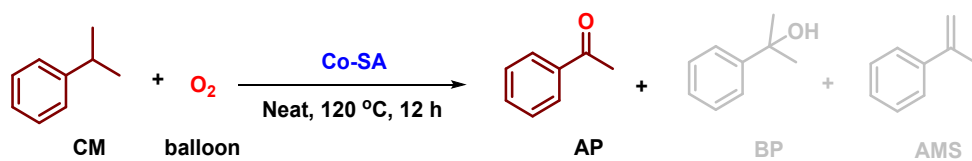
**Table S3.** Screening of Fe single-atom catalyst <sup>ab</sup>



Entry	Catalyst	Conv. (%) <sup>b</sup>
1	Fe <sub>1</sub> @CeO <sub>2</sub>	3.6
2	Fe <sub>1</sub> @ZnO	64
3	Fe <sub>1</sub> @MgO	99
4	Fe <sub>1</sub> @SiO <sub>2</sub>	99
5	Fe <sub>1</sub> @Al <sub>2</sub> O <sub>3</sub>	-
6	Fe <sub>1</sub> @ZrO <sub>2</sub>	6

<sup>a</sup> Fe-SA (40 mg), CM (2.9 mmol, 0.4 mL), 400 rpm; <sup>b</sup> Conversion was determined by GC-MS analysis with internal standard (*n*-dodecane); Conv. = Conversion; “-” means no reaction.

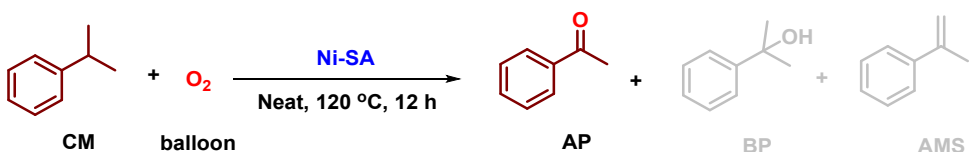
**Table S4.** Screening of Co single-atom catalyst <sup>ab</sup>



Entry	Catalyst	Conv. (%) <sup>b</sup>
1	Co <sub>1</sub> @CeO <sub>2</sub>	64
2	Co <sub>1</sub> @ZnO	73
3	Co <sub>1</sub> @MgO	99
4	Co <sub>1</sub> @SiO <sub>2</sub>	-
5	Co <sub>1</sub> @Al <sub>2</sub> O <sub>3</sub>	-
6	Co <sub>1</sub> @ZrO <sub>2</sub>	44

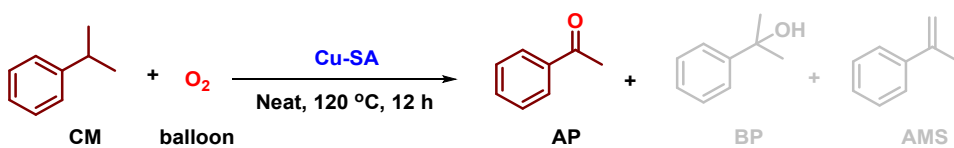
<sup>a</sup> Co-SA (40 mg), CM (2.9 mmol, 0.4 mL), 400 rpm; <sup>b</sup> Conversion was determined by GC-MS analysis with internal standard (*n*-dodecane); Conv. = Conversion; “-” means no reaction.

**Table S5.** Screening of Ni single-atom catalyst <sup>ab</sup>

 <p>CM + O<sub>2</sub> <math>\xrightarrow[\text{Neat, 120 °C, 12 h}]{\text{Ni-SA}}</math> AP + BP + AMS</p>		
Entry	Catalyst	Conv. (%) <sup>b</sup>
1	Ni <sub>1</sub> @CeO <sub>2</sub>	17
2	Ni <sub>1</sub> @ZnO	64
3	Ni <sub>1</sub> @MgO	91
4	Ni <sub>1</sub> @SiO <sub>2</sub>	-
5	Ni <sub>1</sub> @Al <sub>2</sub> O <sub>3</sub>	-
6	Ni <sub>1</sub> @ZrO <sub>2</sub>	-

<sup>a</sup> Ni-SA (40 mg), CM (2.9 mmol, 0.4 mL), 400 rpm; <sup>b</sup> Conversion was determined by GC-MS analysis with internal standard (*n*-dodecane); Conv. = Conversion; “-” means no reaction.

**Table S6.** Screening of Cu single-atom catalyst <sup>ab</sup>

 <p>CM + O<sub>2</sub> <math>\xrightarrow[\text{Neat, 120 °C, 12 h}]{\text{Cu-SA}}</math> AP + BP + AMS</p>		
Entry	Catalyst	Conv. (%) <sup>b</sup>
1	Cu <sub>1</sub> @CeO <sub>2</sub>	15
2	Cu <sub>1</sub> @ZnO	28
3	Cu <sub>1</sub> @MgO	-
4	Cu <sub>1</sub> @SiO <sub>2</sub>	-
5	Cu <sub>1</sub> @Al <sub>2</sub> O <sub>3</sub>	-
6	Cu <sub>1</sub> @ZrO <sub>2</sub>	-

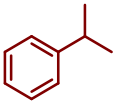

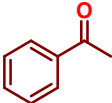
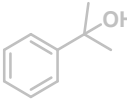
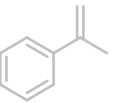
<sup>a</sup> Cu-SA (40 mg), CM (2.9 mmol, 0.4 mL), 400 rpm; <sup>b</sup> Conversion was determined by GC-MS analysis with internal standard (*n*-dodecane); Conv. = Conversion; “-” means no reaction.

**Table S7.** Screening of Zn single-atom catalyst <sup>ab</sup>

CM	balloon	AP BP AMS
Entry	Catalyst	Conv. (%) <sup>b</sup>
1	Zn <sub>1</sub> @CeO <sub>2</sub>	-
2	Zn <sub>1</sub> @ZnO	-
3	Zn <sub>1</sub> @MgO	85
4	Zn <sub>1</sub> @SiO <sub>2</sub>	-
5	Zn <sub>1</sub> @Al <sub>2</sub> O <sub>3</sub>	-
6	Zn <sub>1</sub> @ZrO <sub>2</sub>	-

<sup>a</sup> Zn-SA (40 mg), CM (2.9 mmol, 0.4 mL), 400 rpm; <sup>b</sup> Conversion was determined by GC-MS analysis with internal standard (*n*-dodecane); Conv. = Conversion; “-” means no reaction.

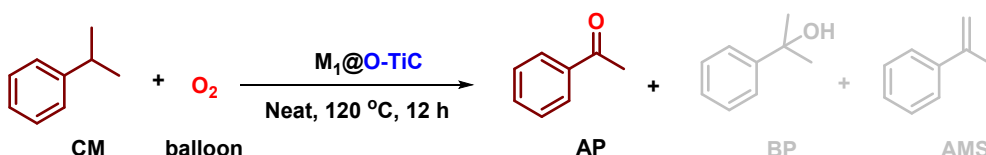
**Table S8.** Investigation of the reaction of TiO<sub>2</sub> loaded with different metals <sup>ab</sup>

	+		$\xrightarrow[\text{Neat, 120 } ^\circ\text{C, 12 h}]{\text{M}_1@\text{TiO}_2}$		+		+	
CM		balloon		AP		BP		AMS
Entry	Catalyst		Conv. (%) <sup>b</sup>					
1	Cr <sub>1</sub> @TiO <sub>2</sub>		-					
2	Mn <sub>1</sub> @TiO <sub>2</sub>		14					
3	Fe <sub>1</sub> @TiO <sub>2</sub>		-					
4	Co <sub>1</sub> @TiO <sub>2</sub>		-					
5	Ni <sub>1</sub> @TiO <sub>2</sub>		91					
6	Cu <sub>1</sub> @TiO <sub>2</sub>		-					
7	Zn <sub>1</sub> @TiO <sub>2</sub>		-					

<sup>a</sup> M<sub>1</sub>@TiO<sub>2</sub> (40 mg), 1 (2.9 mmol, 0.4 mL), 400 rpm; <sup>b</sup> Conversion was determined by GC-MS analysis with internal standard (*n*-dodecane); Conv. = Conversion; “-” means no reaction.



**Table S9.** Investigation of the reaction of O-TiC loaded with different metals <sup>ab</sup>

 <div>CM + O<sub>2</sub> <math>\xrightarrow[\text{Neat, 120 } ^\circ\text{C, 12 h}]{\text{M}_1\text{@O-TiC}}</math> AP + BP + AMS</div>		
Entry	Catalyst	Conv. (%) <sup>b</sup>
1	Cr <sub>1</sub> @O-TiC	28
2	Mn <sub>1</sub> @O-TiC	98
3	Fe <sub>1</sub> @O-TiC	92
4	Co <sub>1</sub> @O-TiC	38
5	Ni <sub>1</sub> @O-TiC	81
6	Cu <sub>1</sub> @O-TiC	98
7	Zn <sub>1</sub> @O-TiC	42
8	Rh <sub>1</sub> @O-TiC	31
9 <sup>c</sup>	O-TiC	20

<sup>a</sup> M<sub>1</sub>@O-TiC (40 mg), CM (2.9 mmol, 0.4 mL), 400 rpm; <sup>b</sup> Conversion was determined by GC-MS analysis with internal standard (*n*-dodecane); <sup>c</sup> O-TiC (50 mg); Conv. = Conversion; “-” means no reaction.

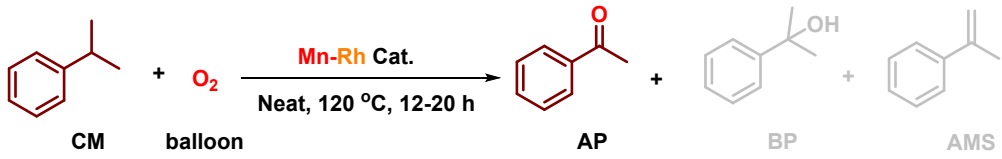
**Table S10.** Investigation of the reaction of TiN loaded with different metals <sup>ab</sup>

CC(C)c1ccccc1 +  $O_2$   $\xrightarrow[\text{Neat, 120 } ^\circ\text{C, 12 h}]{M_1@TiN}$  CC(=O)c1ccccc1 + CC(O)(C)c1ccccc1 + CC(=C)c1ccccc1  
 CM                      balloon                      AP                      BP                      AMS

Entry	Catalyst	Conv. (%) <sup>b</sup>
1	Cr <sub>1</sub> @TiN	-
2	Mn <sub>1</sub> @TiN	97
3	Fe <sub>1</sub> @TiN	-
4	Co <sub>1</sub> @TiN	-
5	Ni <sub>1</sub> @TiN	-
6	Cu <sub>1</sub> @TiN	-
7	Zn <sub>1</sub> @TiN	-

<sup>a</sup> M<sub>1</sub>@TiN (40 mg), CM (2.9 mmol, 0.4 mL), 400 rpm; <sup>b</sup> Conversion was determined by GC-MS analysis with internal standard (*n*-dodecane); Conv. = Conversion; “-” means no reaction.

**Table S11.** Screening of Mn-Rh dual single atom catalyst with different supports<sup>abcd</sup>

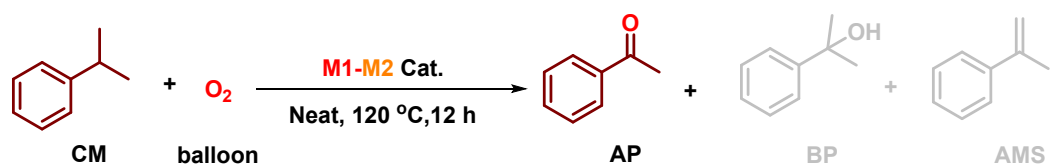


CM + O<sub>2</sub>  $\xrightarrow[\text{Neat, 120 °C, 12-20 h}]{\text{Mn-Rh Cat.}}$  AP + BP + AMS

Entry	Catalyst	Conv. (%) <sup>b</sup>	Sel. (%) <sup>b</sup>
1	Mn <sub>1</sub> -Rh <sub>1</sub> @O-TiC	99	99
2 <sup>c</sup>	Mn <sub>1</sub> -Rh <sub>1</sub> @TiN	47	86
3 <sup>d</sup>	Mn <sub>1</sub> -Rh <sub>1</sub> @TiO <sub>2</sub>	80	96
4	Mn <sub>1</sub> -Rh <sub>1</sub> @O-CrC	29	83
5	Mn <sub>1</sub> -Rh <sub>1</sub> @O-VC	-	-
6	Mn <sub>1</sub> -Rh <sub>1</sub> @O-SiC	31	83
7	Mn-Rh NC/O-TiC	26	45
8	None	-	-

<sup>a</sup> Catalyst (40 mg), CM (2.9 mmol, 0.4 mL), 400 rpm, 12 h; <sup>b</sup> Conversion and selectivity were determined by GC-MS analysis with internal standard (*n*-dodecane); <sup>c</sup> Catalyst (30 mg); <sup>d</sup> Reaction time: 20 h; Conv. = Conversion; Sel. = Selectivity; “-” means no reaction; N.D. = not detected.

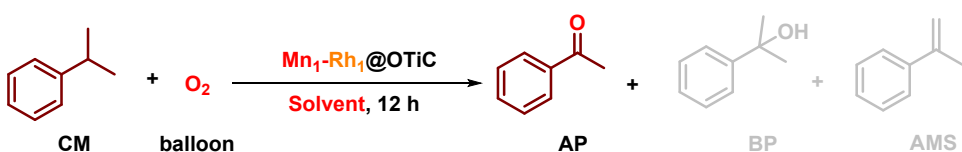
**Table S12.** Screening of dual single atom catalyst <sup>ab</sup>



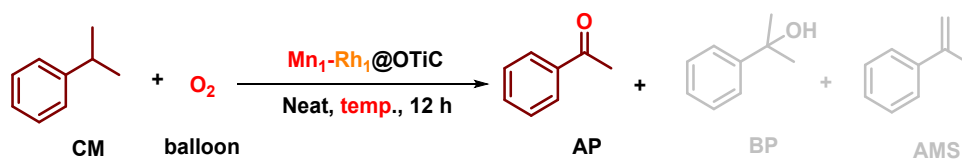
Entry	Catalyst	Conv. (%) <sup>b</sup>	Sel. (%) <sup>b</sup>
1	Mn <sub>1</sub> -Fe <sub>1</sub> @O-TiC	91	38
2	Mn <sub>1</sub> -Cu <sub>1</sub> @O-TiC	-	-
3	Mn <sub>1</sub> -Hf <sub>1</sub> @O-TiC	70	95
4	Mn <sub>1</sub> -Pd <sub>1</sub> @O-TiC	75	97
5	Mn <sub>1</sub> -Ir <sub>1</sub> @O-TiC	79	93
6	Fe <sub>1</sub> -Rh <sub>1</sub> @O-TiC	-	-
7	Cu <sub>1</sub> -Rh <sub>1</sub> @O-TiC	49	80

<sup>a</sup> Catalyst (40 mg), CM (2.9 mmol, 0.4 mL), 400 rpm; <sup>b</sup> Conversion and selectivity were determined by GC-MS analysis with internal standard (*n*-dodecane); Conv. = Conversion; Sel. = Selectivity; “-” means no reaction.

**Table S13.** Screening of solvent <sup>ab</sup>

<div><div><div><div>CM</div><div>balloon</div><div>O<sub>2</sub></div><div>Mn<sub>1</sub>-Rh<sub>1</sub>@OTiC</div><div>Solvent, 12 h</div><div>AP</div><div>BP</div><div>AMS</div></div></div></div>			
Entry	Solvent	Temp. (°C)	Conv. (%) <sup>b</sup>
1	THF	60	-
2	2-MeTHF	80	-
3	Acetonitrile	80	-
4	1,4-dioxane	100	-
5	<i>n</i> -octane	100	-
6	DMF	120	-
7	NMP	120	-
8	H <sub>2</sub> O	100	-

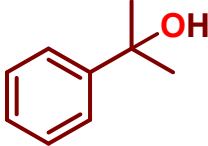
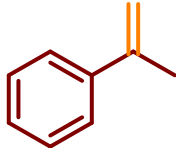
<sup>a</sup> Mn<sub>1</sub>-Rh<sub>1</sub>@O-TiC (10 mg), CM (0.24 mmol, 28.8 mg, 33 uL), 800 rpm, 12 h; <sup>b</sup> Conversion was determined by GC-MS analysis with internal standard (*n*-dodecane) ; “-” means no reaction.

**Table S14.** Screening of reaction temperature and other conditions <sup>abcdefg</sup>

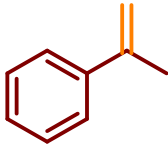
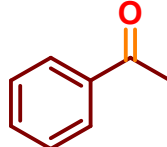
Entry	Temp. (°C)	Conv. (%) <sup>b</sup>	Sel. (%) <sup>b</sup>
1	60	37	93
2	80	46	95
3	100	80	95
4	110	91	97
5	120	99	99
6 <sup>c</sup>	120	99	99
7 <sup>d</sup>	120	84	99
8 <sup>e</sup>	120	99	99
9 <sup>f</sup>	120	-	-
10 <sup>g</sup>	120	-	-
11	130	99	99

<sup>a</sup> Mn<sub>1</sub>-Rh<sub>1</sub>@O-TiC (40 mg, 0.08 mmol%), CM (2.9 mmol, 0.4 mL), 400 rpm, 12 h; <sup>b</sup> Conversion and selectivity were determined by GC-MS analysis with internal standard (n-dodecane); <sup>c</sup> Prolonged to 20 h; <sup>d</sup> Catalyst (30 mg, 0.06 mol%); <sup>e</sup> Catalyst (50 mg, 0.1 mol%); <sup>f</sup> under Air; <sup>g</sup> under Ar; Conv. = Conversion; Sel. = Selectivity; “-” means no reaction.

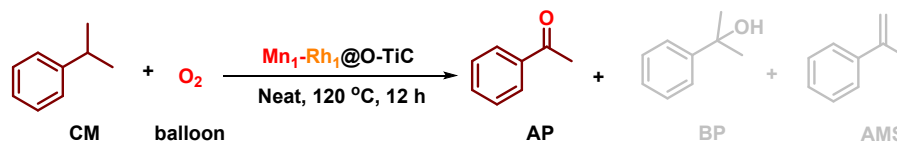
**Table S15.** Comparative results of BP dehydration

	$\xrightarrow[\text{Neat, 120 } ^\circ\text{C, 24 h}]{\text{Catalyst}}$	
BP		AMS
Entry	Catalyst (40 mg)	Yield (%)
1	$\text{Rh}_1\text{@O-TiC}$	25
2	$\text{Mn}_1\text{@O-TiC}$	5.4
3	O-TiC	0

**Table S16.** Comparative results of AMS oxidative cracking

	$\xrightarrow[\text{Neat, 120 } ^\circ\text{C, 24 h}]{\begin{array}{c} \text{Rh}_1\text{@O-TiC} \\ \text{or} \\ \text{Mn}_1\text{@O-TiC} \\ \text{O}_2 \text{ (1 atm)} \end{array}}$	
AMS		AP
Entry	Catalyst (40 mg)	Yield (%)
1	$\text{Rh}_1\text{@O-TiC}$	30
2	$\text{Mn}_1\text{@O-TiC}$	33

**Table S17.** Effect of physical milling ratio of Mn<sub>1</sub>@O-TiC and Rh<sub>1</sub>@O-TiC on the reaction

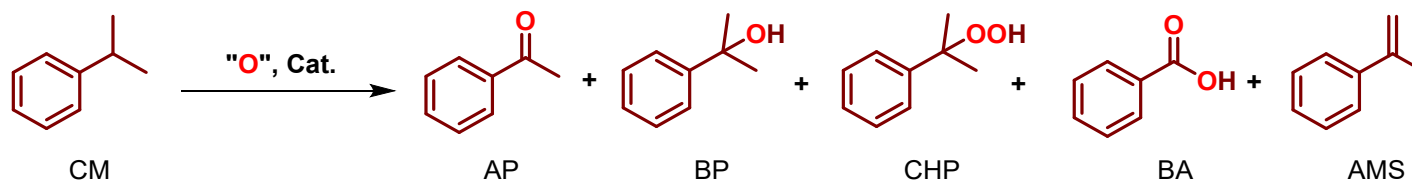


Entry	Mn <sub>1</sub> @O-TiC (mg)	Rh <sub>1</sub> @O-TiC (mg)	Conv. (%)	Sel. (%) <sup>b</sup>
1	100	100	52	91
2	100	50	59	92
3	100	20	66	96
4	100	10	99	99
5	50	100	60	92
6	20	100	55	85
7	10	100	48	85

<sup>a</sup> Mn<sub>1</sub>-Rh<sub>1</sub>@O-TiC (40 mg), CM (2.9 mmol, 0.4 mL), 400 rpm, 12 h; <sup>b</sup> Conversion and selectivity were determined by GC-MS analysis with internal standard (*n*-dodecane); Conv. = Conversion; Sel. = Selectivity.



**Table S18.** Comparison of catalytic performance in cumene oxidation over different catalysts.



Author	Catalyst	"O" source	Reaction conditions	Conv. (%)	Sel. (%) or Yield (%)					TON	Ref
					AP	BP	CHP	BA	AMS		
Yang, C.-J., et al.	(0.08 mol%) Mn <sub>1</sub> -Rh <sub>1</sub> @O-TiC	O <sub>2</sub> (1atm)	Neat, 120 °C, 12 h	99	99	-	-	-	1	1152	This work
Zhu, H.-F., et al.	g-C <sub>3</sub> N <sub>4</sub> -2	O <sub>2</sub> (1atm)	10 w white light CHP, 20 h	23.02	0.86	16.92	82.22	-	-	-	5
Chen, Z.-C., et al.	Co-N-C	O <sub>2</sub> (25mL·min <sup>-1</sup> )	80 °C, 8 h	49.76	9.03	65.22	25.75	-	-	-	6
Deng, Y.-C., et al.	21.23-MnO <sub>2</sub> /CNTs	O <sub>2</sub> (25 mL·min <sup>-1</sup> )	80 °C, 7 h	73.44	30.63	59.06	10.30	-	-	-	7
Chen, Z.-C., et al.	CNTs	O <sub>2</sub> (25 mL·min <sup>-1</sup> )	80 °C, 8 h	56.1	4.5	51.1	44.4	-	-	-	8
Zhang, G.-X., et al.	FeCl <sub>3</sub>	O <sub>2</sub> (1atm)	390 nm, 100 w, 126 h					57			9
Shen, H.-M., et al.	TPFPpCo	O <sub>2</sub> (1atm)	8 h	57.4	22	46.4	31.6	22	-	-	10

Inoa, J., et al.	Eosin Y	O <sub>2</sub> (1atm)	blue LEDs, 10 h				83				11
Nowacka, A., et al.	Co-BTC	O <sub>2</sub> (4 bar)	90 °C, 7 h	49	-	-	69	-	-	-	12
Maurya, M., et al.	V <sup>V</sup> O <sub>2</sub> -complex	30% H <sub>2</sub> O <sub>2</sub>	20 h	61	80					61	13
Liu, W.-G., et al.	Fe-N-C-700	TBHP	H <sub>2</sub> O, 7 h	99	-	80	-	-	-	150	14
Liu, H.-S., et al.	L <sub>0.8</sub> -C <sub>0.03</sub> -M <sub>1</sub>	O <sub>2</sub> (4 bar)	90 °C, 6 h	95.5	1.75	36.23	60.57	-	-	-	15
Kasperczyk, K., et al.	NHPI	O <sub>2</sub> (1atm )	AIBN, 60 °C, 6 h	50	-	-	100	-	-	-	16
Mu, C.-L., et al.	CNT/Al <sub>2</sub> O <sub>3</sub> /Ni	O <sub>2</sub> (4 bar)	80 °C, 8 h	25.1	0.7	6.0	15.8				17
Wang, F.-F., et al.	CuO@Cu <sub>3</sub> (BTC) <sub>2</sub>	Air	CHP, 110 °C, 12 h				18.1				18
Xu, S., et al.	[C <sub>4</sub> dmim]Br	O <sub>2</sub> (10 mL·min <sup>-1</sup> )	80 °C, 8 h	66.6	4.1	53.1	-	-	-	-	19
Wang, M., et al.	FeCl <sub>2</sub>	O <sub>2</sub> (1atm)	50 W LED, 24 h					51			20
J. C. Scaiano., et al.	AgNP@HT	O <sub>2</sub> (1atm)	80 °C, 8 h			2.4	9.4				21
Chen, Z.-C., et al.	CNTs	O <sub>2</sub> (25 mL·min <sup>-1</sup> )	80 °C, 8 h	41.8	4.1	24.4	75.1	-	-	-	22
Ma, D. et al.	LC-N-8.9	O <sub>2</sub> (4 MPa)	TBHP, 100 °C, 48 h	97	22.7	77.3	-	-	-	-	23
Zhou, A. W. et al.	GVL	O <sub>2</sub>	140 °C, 24 h	99	56	-	-	-	-	-	24

**Note: The blue markers in the above table are the isolated yields of the products.**

**Table S19.** The ICP test of the Mn<sub>1</sub>-Rh<sub>1</sub>@O-TiC before and after the reaction.

Element	Before the reaction (wt %)	After the 5 h reaction (wt %)	After the 3 <sup>th</sup> reaction (wt %)
Mn	0.93	0.91	0.90
Rh	0.61	0.61	0.60

**Table S20.** EXAFS fitting parameters at the Rh *K*-edge for various samples ( $S_0^2 = 0.750$ ).

Sample	Shell	$CN^a$	$R(\text{\AA})^b$	$\sigma^2(\text{\AA}^2)^c$	$\Delta E_0(\text{eV})^d$	<i>R</i> factor
Rh foil	Rh-Rh	12	2.68±0.01	0.0029	3.2	0.0077
Rh <sub>2</sub> O <sub>3</sub>	Rh-O	4.6±0.3	2.03±0.01	0.0011	11.4	0.0046
Mn <sub>1</sub> -Rh <sub>1</sub> @O-TiC	Rh-O	4.0±0.3	2.02±0.01	0.0023	9.3	0.0059

<sup>a</sup> $CN$ , coordination number; <sup>b</sup> $R$ , distance between absorber and backscatter atoms; <sup>c</sup> $\sigma^2$ , Debye-Waller factor to account for both thermal and structural disorders; <sup>d</sup> $\Delta E_0$ , inner potential correction; *R* factor indicates the goodness of the fit.  $S_0^2$  was fixed to 0.750, according to the experimental EXAFS fit of Rh foil by fixing  $CN$  as the known crystallographic value. A reasonable range of EXAFS fitting parameters:  $0.600 < S_0^2 < 1.000$ ;  $CN > 0$ ;  $\sigma^2 > 0 \text{ \AA}^2$ ;  $|\Delta E_0| < 15 \text{ eV}$ ; *R* factor  $< 0.02$ .

**Table S21.** EXAFS fitting parameters at the Mn *K*-edge for various samples ( $S_0^2 = 0.910$ ).

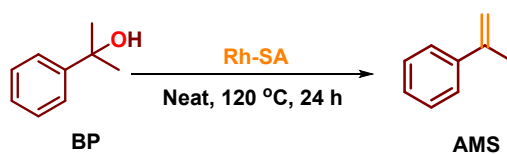
Sample	Shell	CN <sup>a</sup>	<i>R</i> (Å) <sup>b</sup>	$\sigma^2$ (Å <sup>2</sup> ) <sup>c</sup>	$\Delta E_0$ (eV) <sup>d</sup>	<i>R</i> factor
MnPc	Mn-N	4	1.91±0.05	3.6±3.9	-5.6±2.8	0.026
Mn <sub>1</sub> -Rh <sub>1</sub> @O-TiC	Mn-O	3.3±0.7	2.10±0.08	1.9±5.3	0.6±1.7	0.012

The obtained XAFS data was processed in Athena (version 0.9.26) for background, pre-edge line and post-edge line calibrations. Then Fourier transformed fitting was carried out in Artemis (version 0.9.26). The  $k^2$  weighting,  $k$ -range of 2.2 -11.3 Å<sup>-1</sup> and  $R$  range of 1 - ~2.1 Å were used for the fitting of MnPc; Mn sample :  $k$ -range of 1.7-8.3 Å<sup>-1</sup> and  $R$  range of 1-2.3 Å were used for the fitting of samples. The four parameters, coordination number, bond length, Debye-Waller factor and  $E_0$  shift ( $CN$ ,  $R$ ,  $\Delta E_0$ ,  $\sigma^2$ ) were fitted without anyone was fixed.

**Table S22** Effect of nanocatalysts on the reaction <sup>ab</sup>

Ctalyst	<sup>b</sup> Conv. (%)	<sup>b</sup> Sel. (%)
Mn NP/O-TiC	17	32
Rh NP/O-TiC	-	-

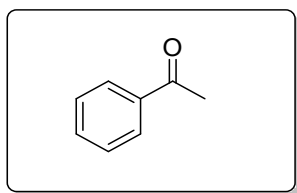
<sup>a</sup> Catalyst (40 mg), CM (2.9 mmol, 0.4 mL), 400 rpm, 12 h; <sup>b</sup> Conversion and selectivity were determined by GC-MS analysis with internal standard (*n*-dodecane); Conv. = Conversion; Sel. = Selectivity; “-” means no reaction.

**Table S23** Screening of Rh single-atom catalyst for BP dehydration <sup>ab</sup>

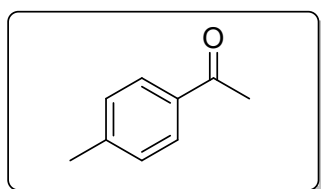
Entry	Catalyst	Yield (%) <sup>b</sup>
1	Rh <sub>1</sub> @O-TiC	25
2	Rh <sub>1</sub> @TiC	18
3	Rh <sub>1</sub> @TiO <sub>2</sub>	4.3
4	Rh <sub>1</sub> @TiN	7.2
5	Rh <sub>1</sub> @ZrO <sub>2</sub>	4
6	Rh <sub>1</sub> @MgO	7.3
7	Rh <sub>1</sub> @Al <sub>2</sub> O <sub>3</sub>	8
8	Rh <sub>1</sub> @O-ZrC	11

<sup>a</sup> Catalyst (40 mg), CM (2.9 mmol, 0.4 mL), 400 rpm, 12 h; <sup>b</sup> Yield was determined by GC-MS analysis with internal standard (*n*-dodecane).

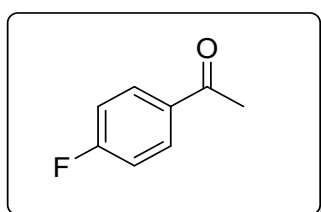
## 5. $^1\text{H}$ , $^{13}\text{C}$ and $^{19}\text{F}$ NMR data of all products



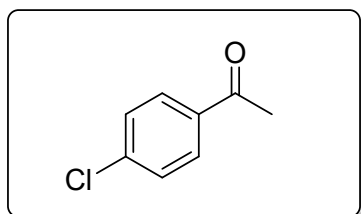
**Acetophenone 2a:** pale yellow liquid. Petroleum ether/ethyl acetate = 30:1 (v/v) as eluent for column chromatography.  $^1\text{H}$  NMR (500 MHz, Chloroform-*d*)  $\delta$  7.87 (dd,  $J$  = 8.4, 1.4 Hz, 2H), 7.52-7.44 (m, 1H), 7.37 (dd,  $J$  = 8.4, 7.1 Hz, 2H), 2.50 (s, 3H).  $^{13}\text{C}$  NMR (126 MHz, Chloroform-*d*)  $\delta$  197.9, 136.9, 132.9, 128.4, 128.1, 26.4.



**4'-Methylacetophenone 2b:** pale yellow liquid. Petroleum ether/ethyl acetate = 30:1 (v/v) as eluent for column chromatography.  $^1\text{H}$  NMR (500 MHz, Chloroform-*d*)  $\delta$  7.81 (d,  $J$  = 8.3 Hz, 2H), 7.20-7.18 (m, 2H), 2.51 (s, 3H), 2.35 (s, 3H).  $^{13}\text{C}$  NMR (126 MHz, Chloroform-*d*)  $\delta$  197.7, 143.9, 134.8, 129.3, 128.5, 26.5, 21.6.

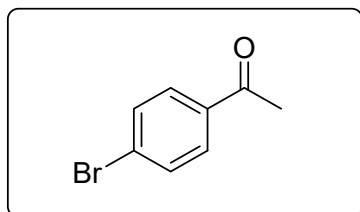


**4-Fluoroacetophenone 2c:** pale yellow liquid. Petroleum ether/ethyl acetate = 30:1 (v/v) as eluent for column chromatography.  $^1\text{H}$  NMR (500 MHz, Chloroform-*d*)  $\delta$  7.93 (dd,  $J$  = 8.9, 5.4 Hz, 2H), 7.07 (t,  $J$  = 8.6 Hz, 2H), 2.54 (s, 3H).  $^{13}\text{C}$  NMR (126 MHz, Chloroform-*d*)  $\delta$  196.7, 167.0, 165.0, 133.9 (d,  $J$  = 3.0 Hz), 131.2 (d,  $J$  = 9.3 Hz), 116.0, 115.8, 26.7.  $^{19}\text{F}$  NMR (471 MHz, Chloroform-*d*)  $\delta$  -105.42.

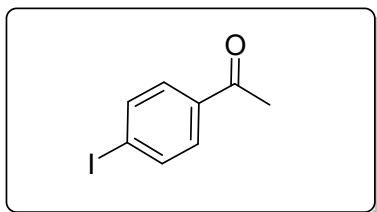




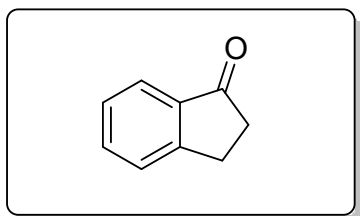
**4'-Chloroacetophenone 2d:** pale yellow liquid. Petroleum ether/ethyl acetate = 30:1 (v/v) as eluent for column chromatography.  $^1\text{H NMR}$  (500 MHz, Chloroform-*d*)  $\delta$  7.76 (d,  $J$  = 8.6 Hz, 2H), 7.28 (d,  $J$  = 8.6 Hz, 2H), 2.46 (s, 3H).  $^{13}\text{C NMR}$  (126 MHz, Chloroform-*d*)  $\delta$  196.6, 139.4, 135.4, 129.7, 128.8, 26.5.



**4'-Bromoacetophenone 2e:** white solid. Petroleum ether/ethyl acetate = 30:1 (v/v) as eluent for column chromatography. m.p.: 108-109 °C.  $^1\text{H NMR}$  (500 MHz, Chloroform-*d*)  $\delta$  7.80 (d,  $J$  = 8.5 Hz, 2H), 7.59 (d,  $J$  = 8.5 Hz, 2H), 2.57 (s, 3H).  $^{13}\text{C NMR}$  (126 MHz, Chloroform-*d*)  $\delta$  197.4, 136.1, 132.2, 130.2, 128.6, 26.9.

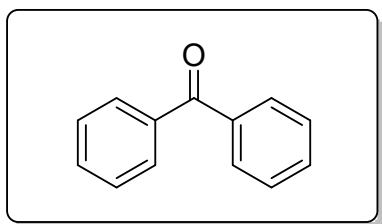


**4'-Iodoacetophenone 2f:** pale yellow liquid. Petroleum ether/ethyl acetate = 30:1 (v/v) as eluent for column chromatography.  $^1\text{H NMR}$  (500 MHz, Chloroform-*d*)  $\delta$  7.82 (d,  $J$  = 8.5 Hz, 2H), 7.66 (d,  $J$  = 8.5 Hz, 2H), 2.57 (s, 3H).  $^{13}\text{C NMR}$  (126 MHz, Chloroform-*d*)  $\delta$  197.7, 138.3, 136.7, 130.1, 101.49, 26.87.

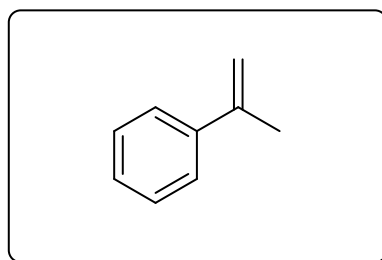


**2,3-Dihydro-1H-inden-1-one 2g:** white solid. Petroleum ether/ethyl acetate = 20:1 (v/v) as eluent for column chromatography. m.p.: 39-41 °C.  $^1\text{H NMR}$  (500 MHz, Chloroform-*d*)  $\delta$  7.71 (d,  $J$  = 7.7 Hz, 1H), 7.53 (dd,  $J$  = 7.4, 1.2 Hz, 1H), 7.44 (dt,  $J$  = 7.7, 1.0 Hz, 1H), 7.33 (d,  $J$  = 7.9 Hz, 1H), 3.11-3.08 (m, 2H), 2.65-2.62 (m, 2H).  $^{13}\text{C NMR}$

**NMR** (126 MHz, Chloroform-*d*)  $\delta$  206.8, 154.9, 136.8, 134.4, 127.0, 126.5, 123.4 , 35.9, 25.5.



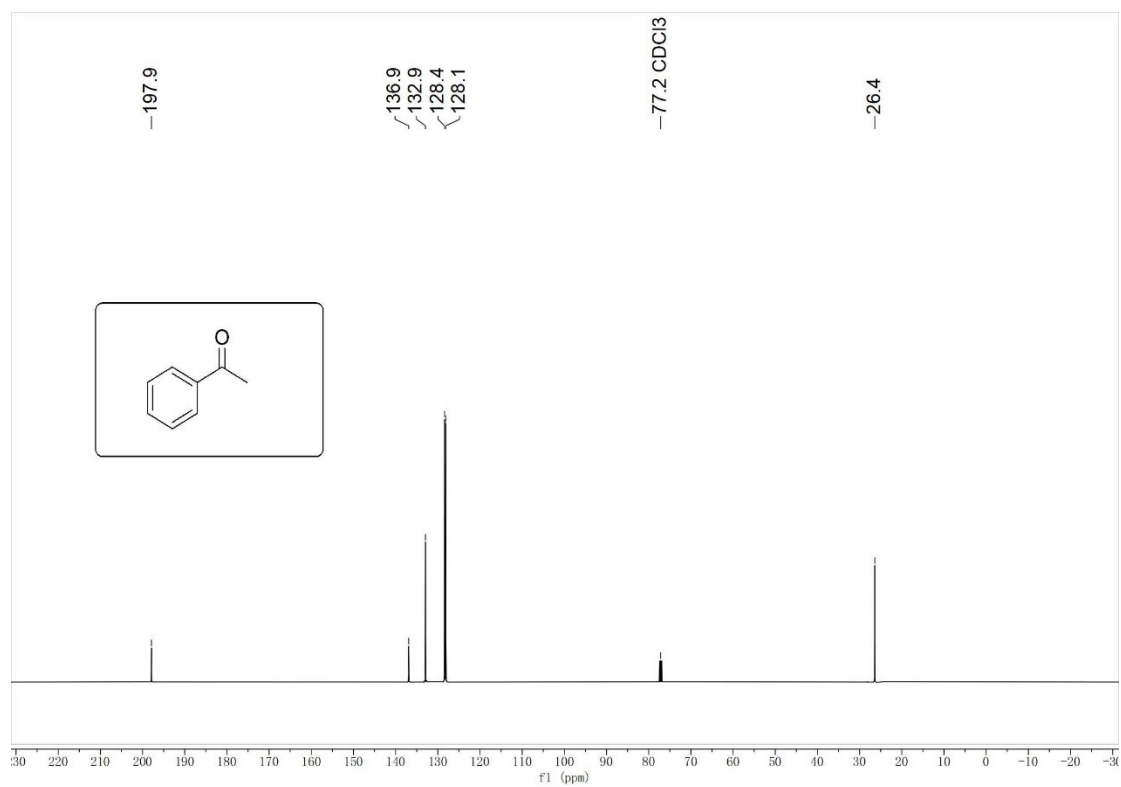
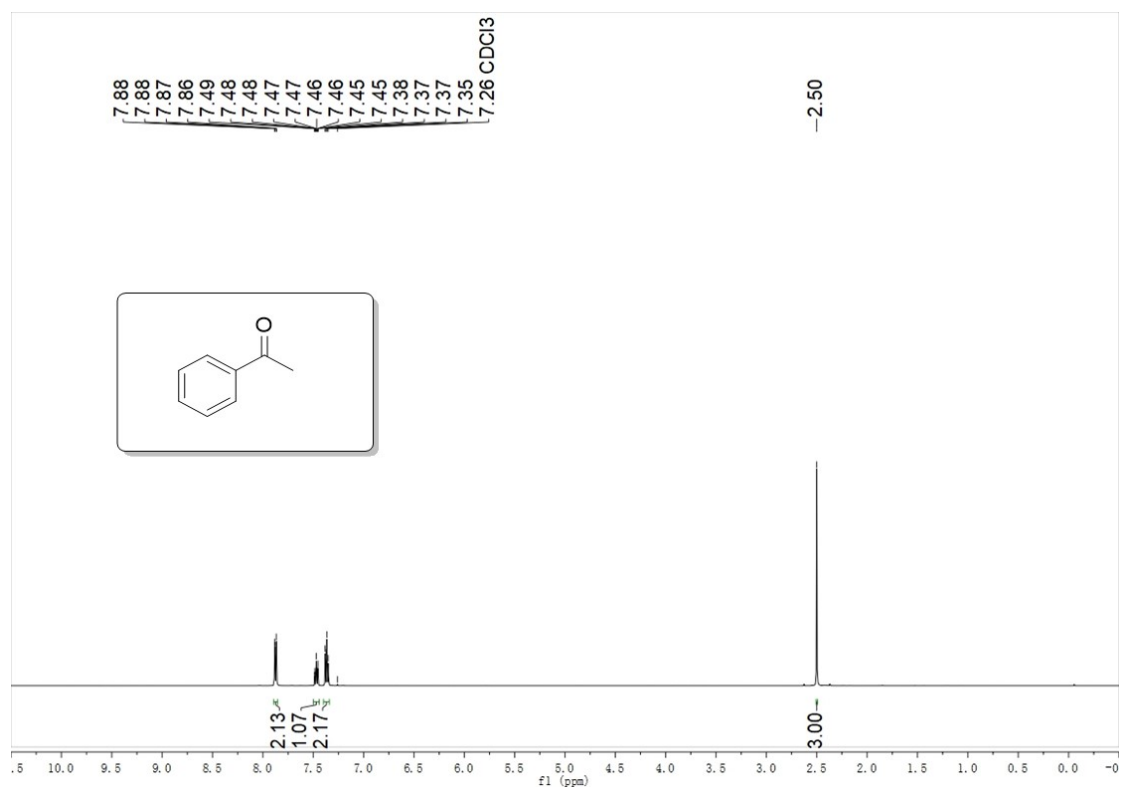
**Benzophenone 2h**: white powder. Petroleum ether/ethyl acetate = 20:1 (v/v) as eluent for column chromatography. m.p.: 48-52 °C. **<sup>1</sup>H NMR** (500 MHz, Chloroform-*d*)  $\delta$  7.82-7.80 (m, 4H), 7.60-7.57 (m, 2H), 7.50-7.46 (m, 4H). **<sup>13</sup>C NMR** (126 MHz, Chloroform-*d*)  $\delta$  196.6, 137.4, 132.3, 129.9, 128.1.



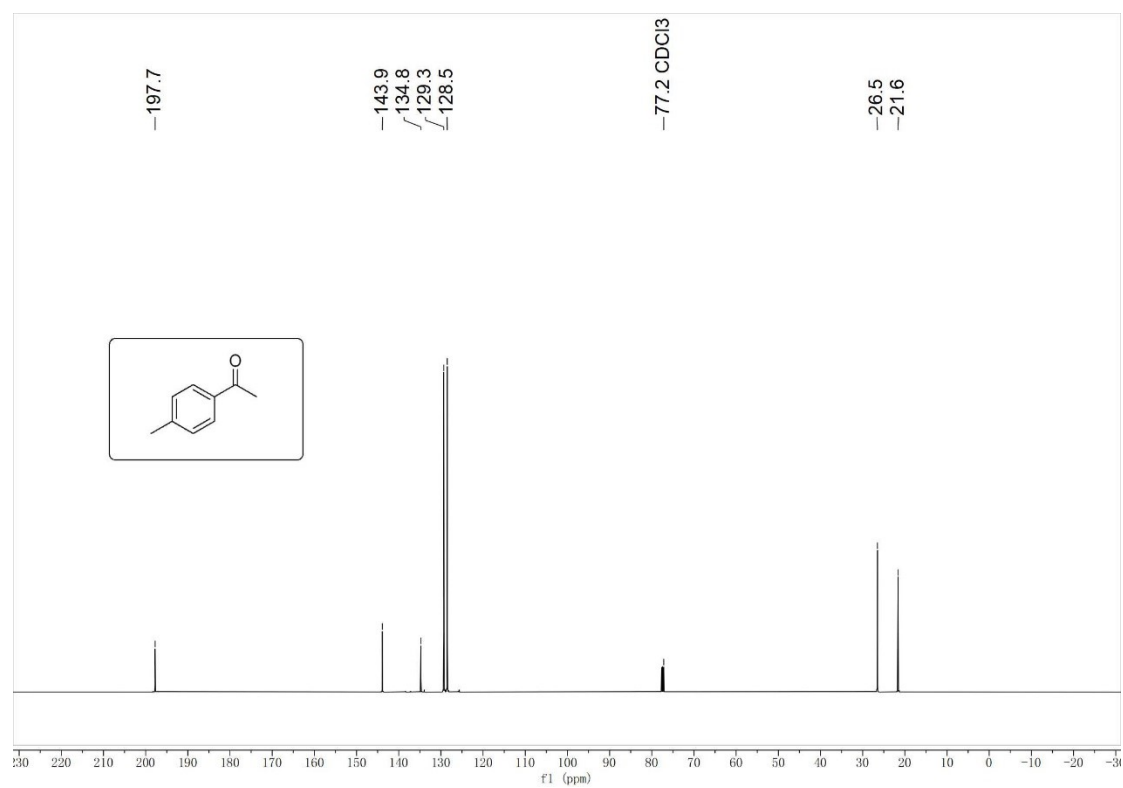
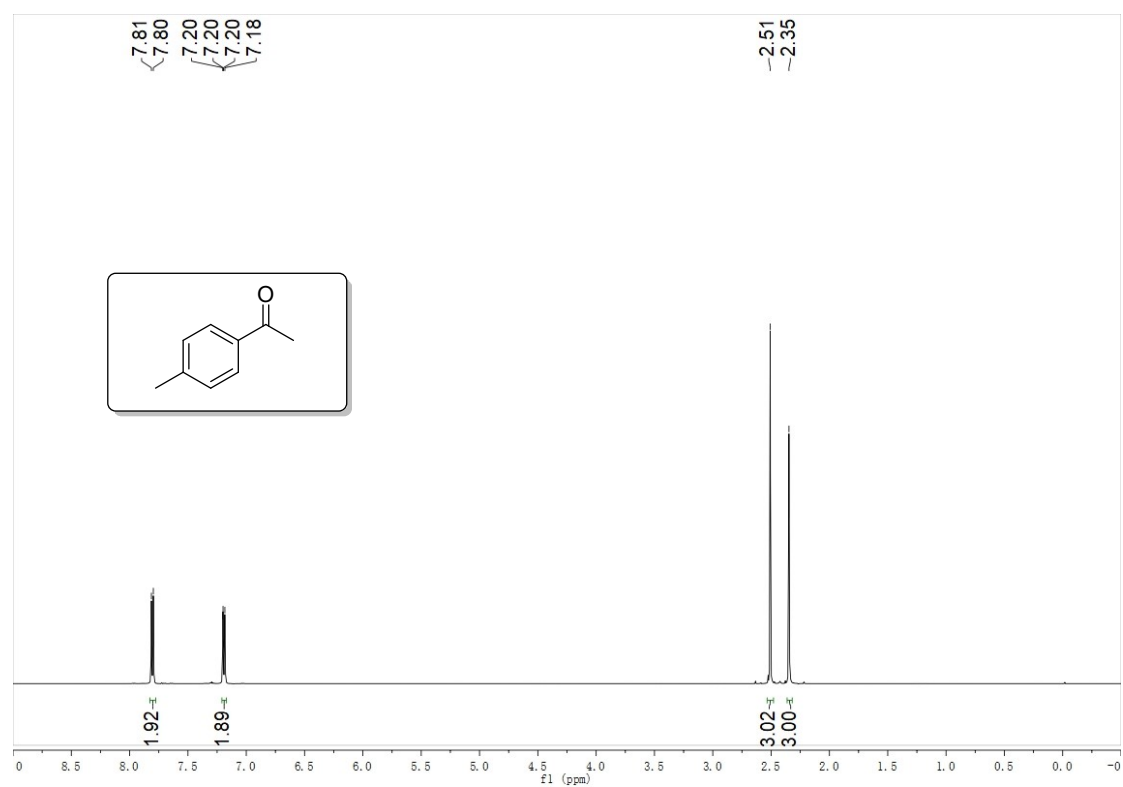
**$\alpha$ -Methyl styrene (AMS)**: colourless liquid. Petroleum ether as eluent for column chromatography. **<sup>1</sup>H NMR** (400 MHz, Chloroform-*d*)  $\delta$  7.48-7.45 (m, 2H), 7.34-7.30 (m, 2H), 7.28-7.25 (m, 1H), 5.37 (dd,  $J$  = 1.6, 0.8 Hz, 1H), 5.08 (t,  $J$  = 1.6 Hz, 1H), 2.15 (s, 3H). **<sup>13</sup>C NMR** (101 MHz, Chloroform-*d*)  $\delta$  143.1, 141.0, 128.0, 127.2, 125.3, 112.24, 21.6.

## 6. Copies of $^1\text{H}$ , $^{13}\text{C}$ and $^{19}\text{F}$ NMR spectra for products

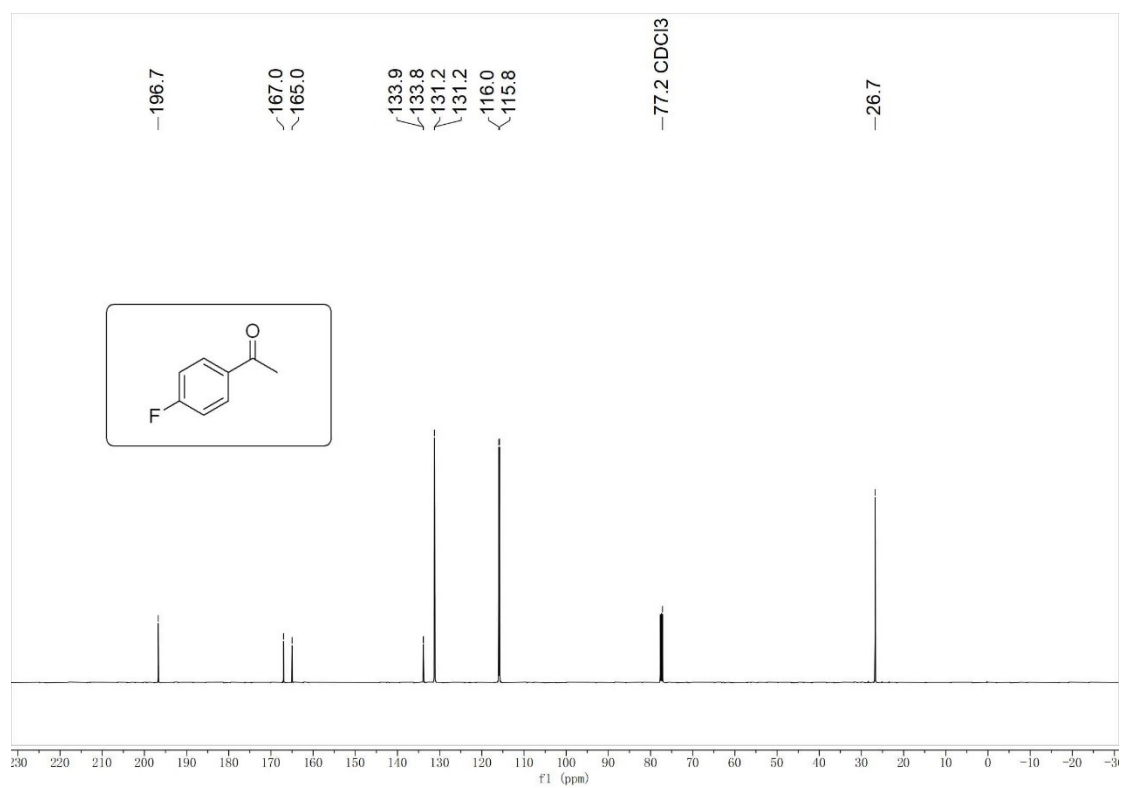
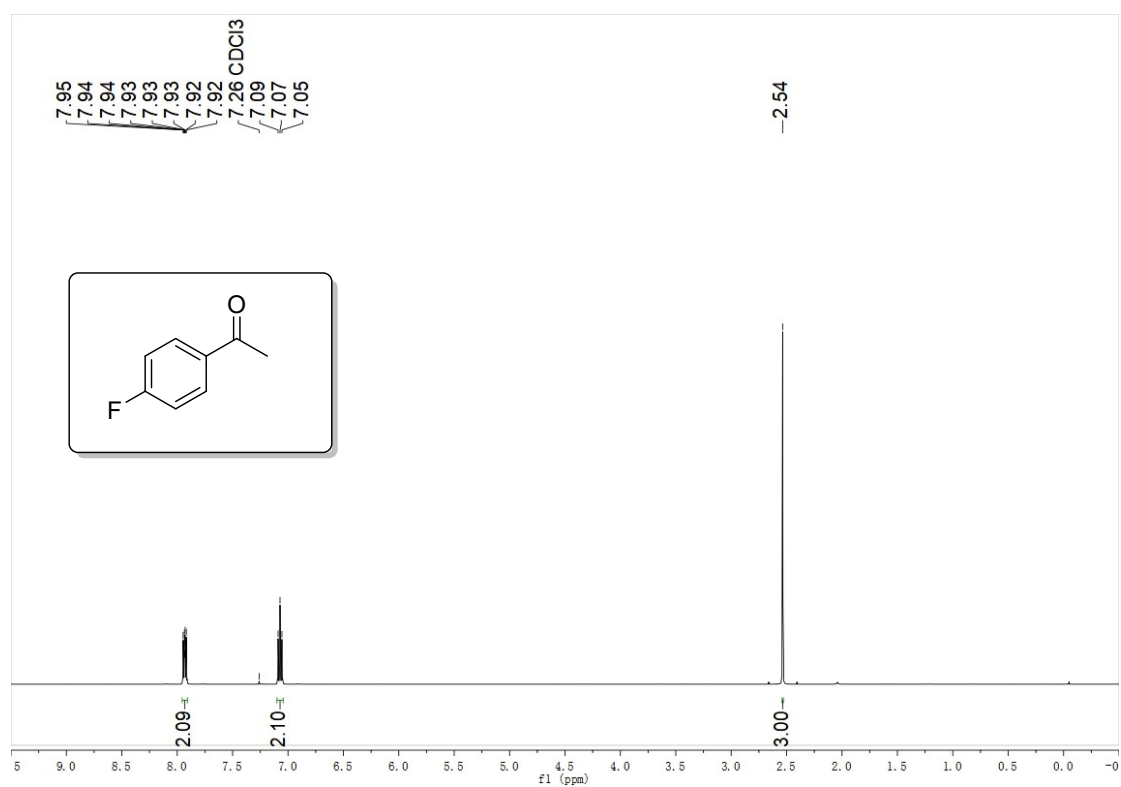
### Acetophenone (2a)



# 4'-Methylacetophenone (**2b**)

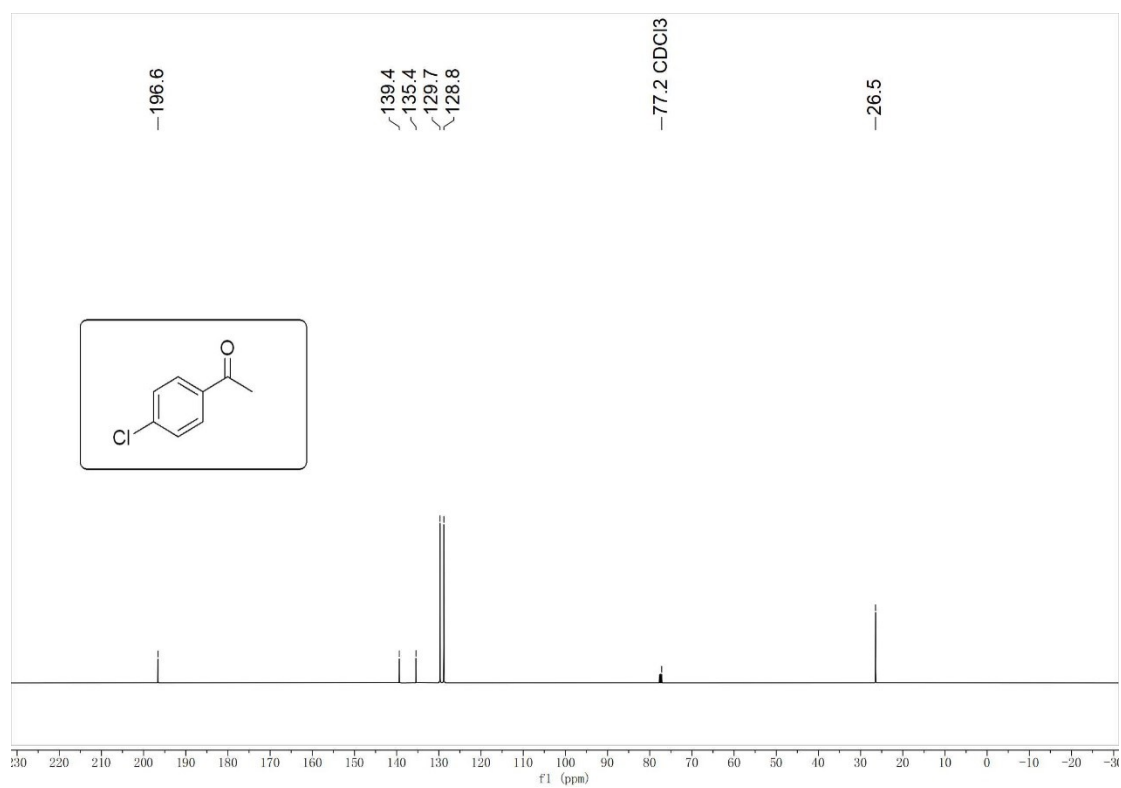
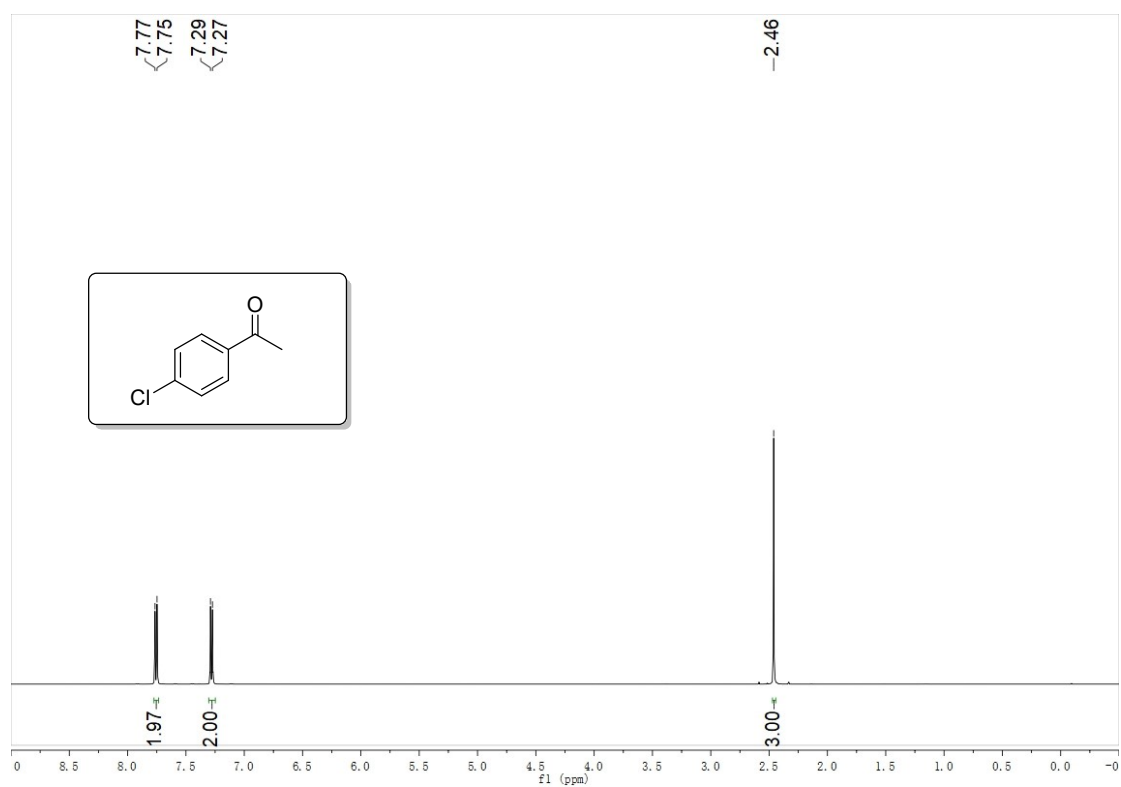


# 4-Fluoroacetophenone (**2c**)

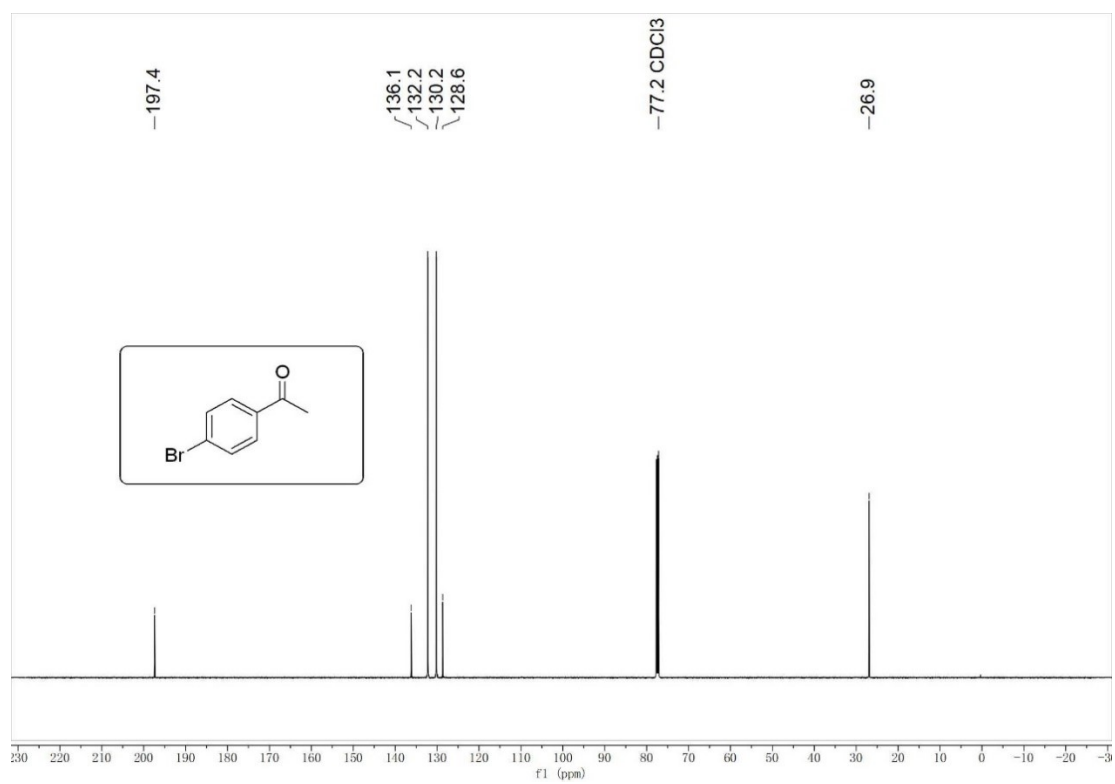




# 4'-Chloroacetophenone (**2d**)

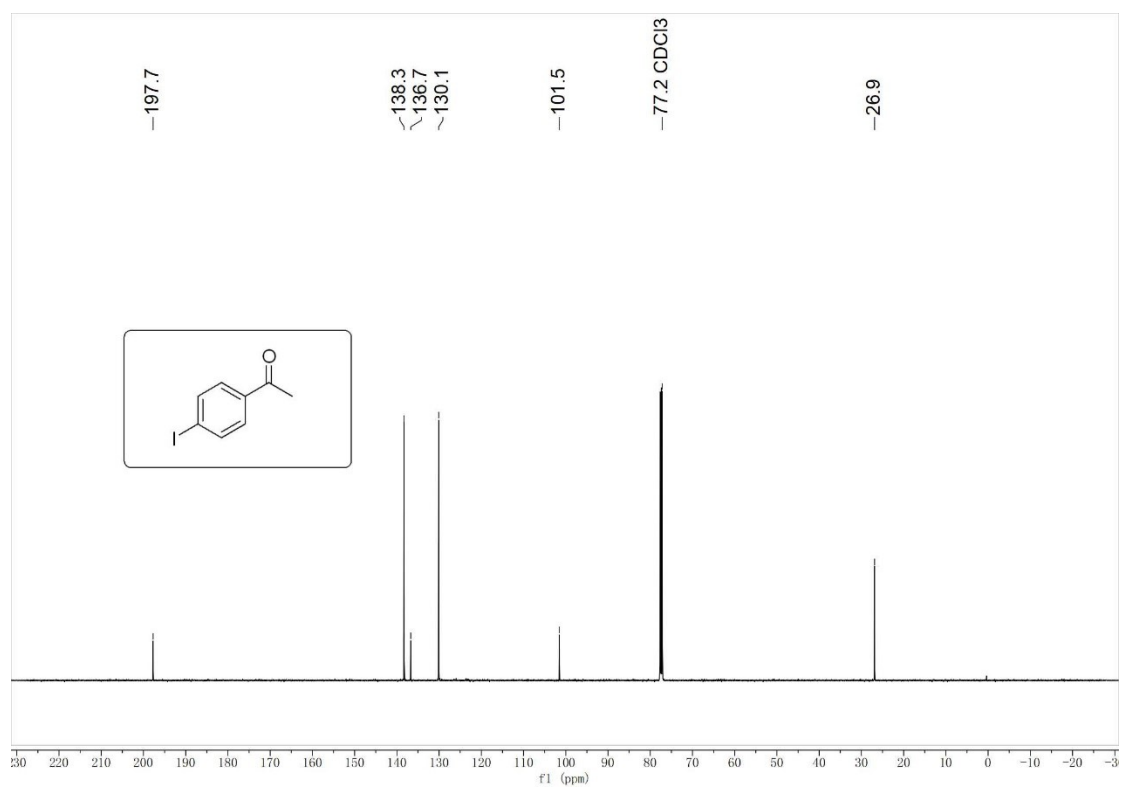
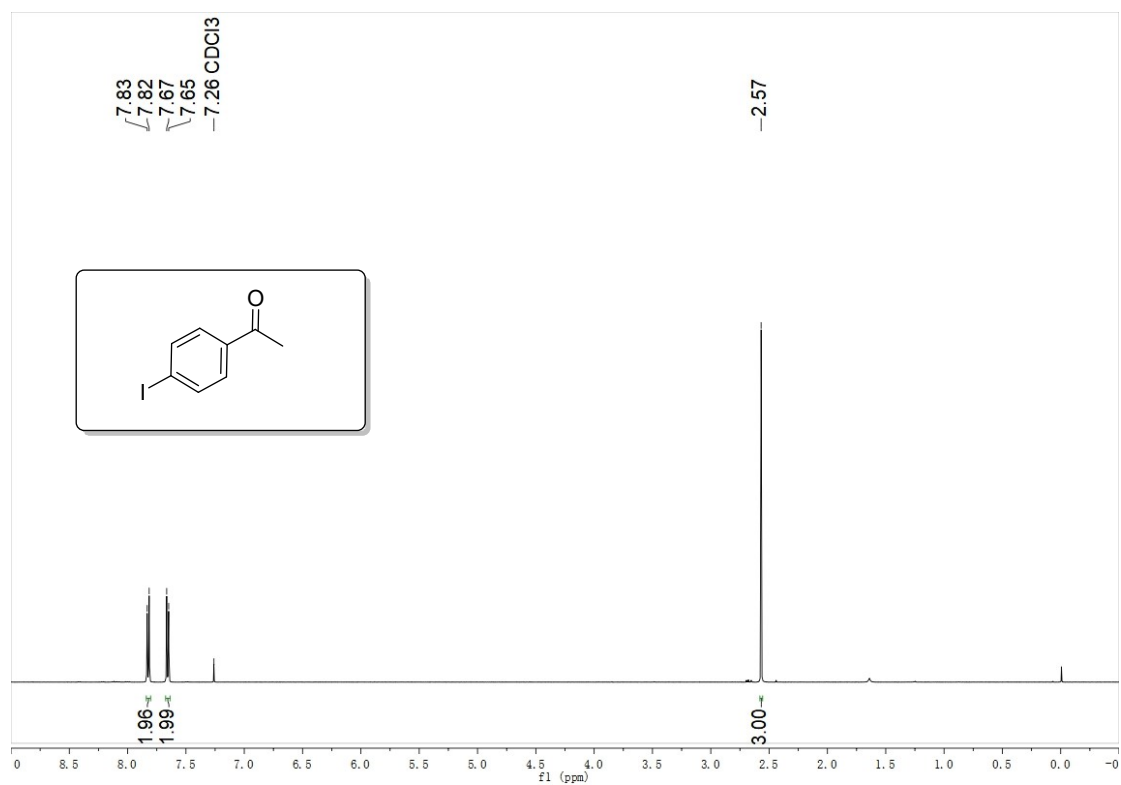


# 4'-Bromoacetophenone (**2e**)

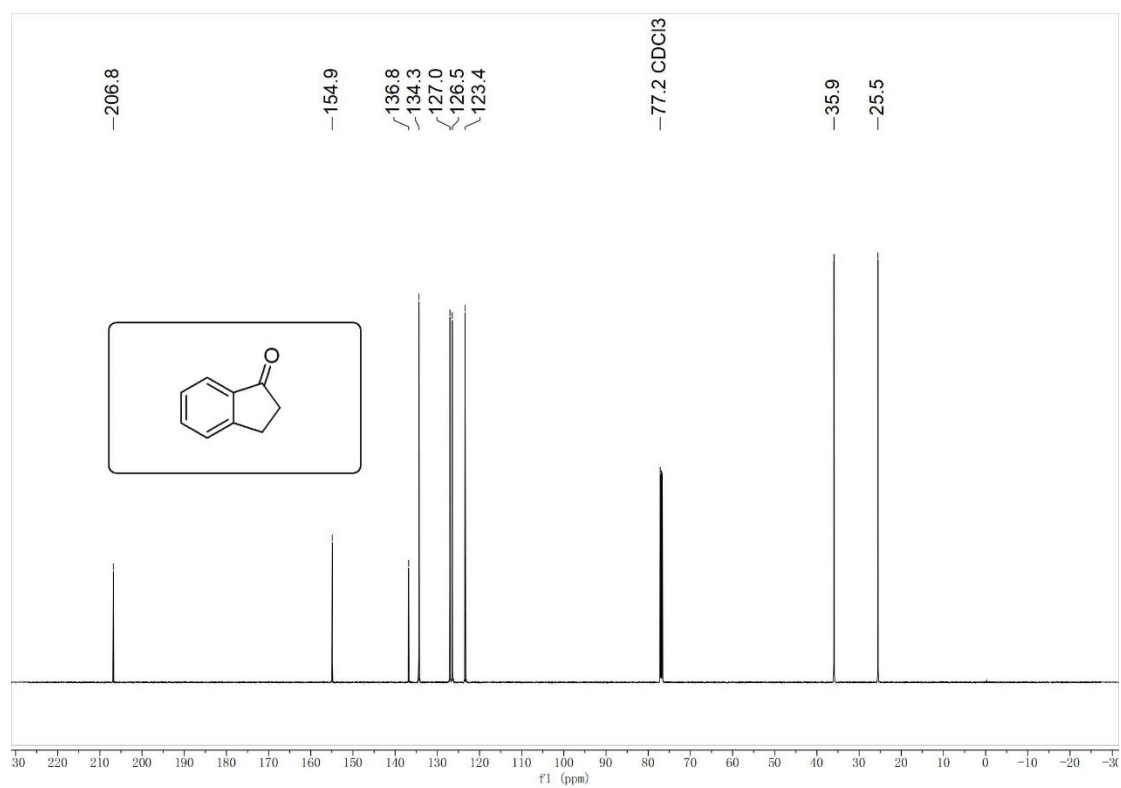
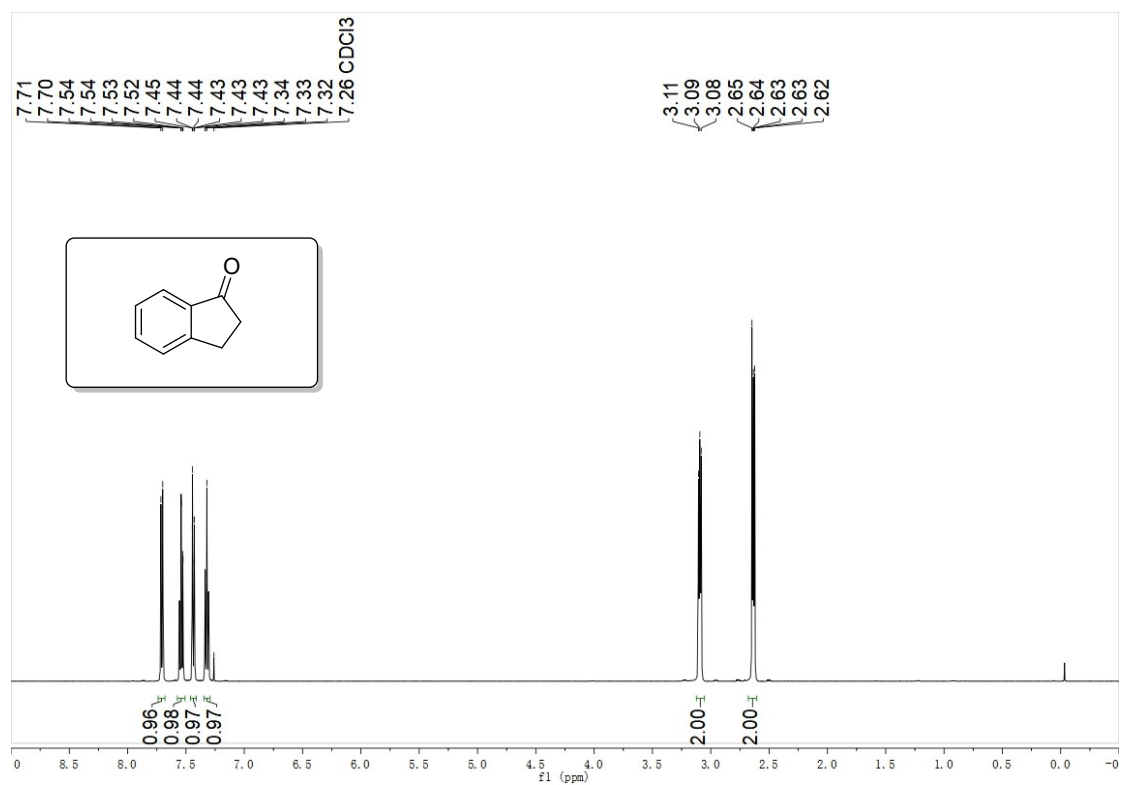




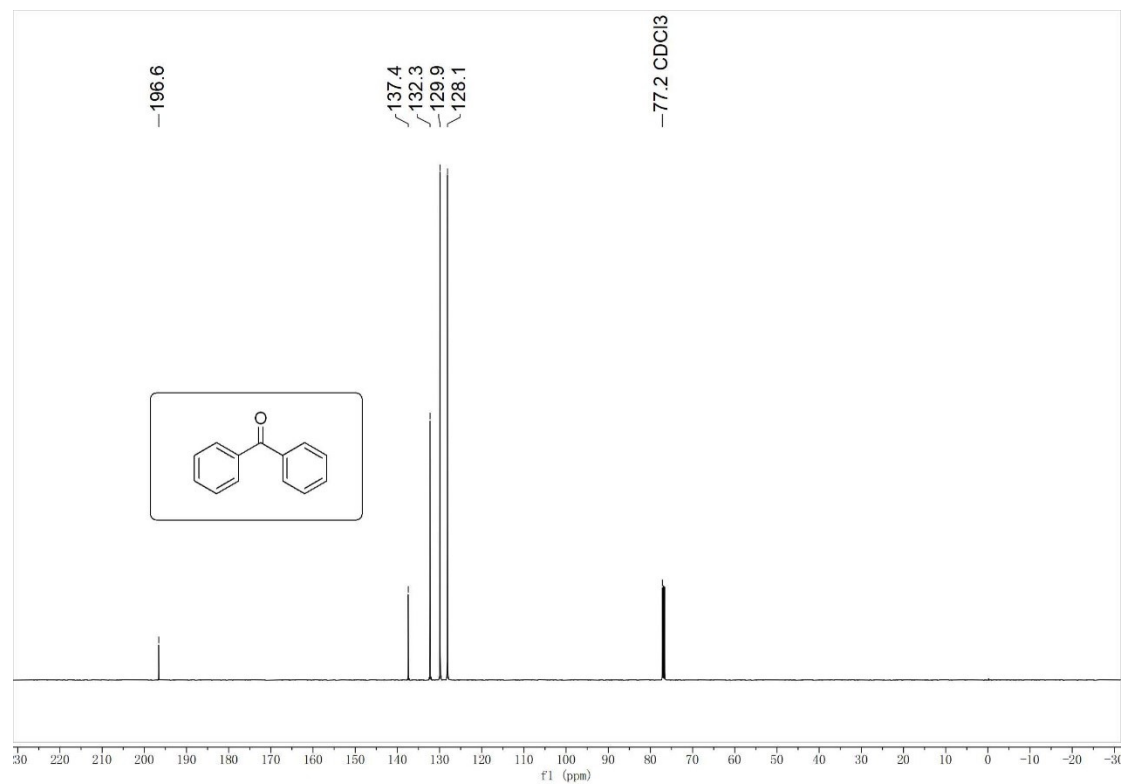
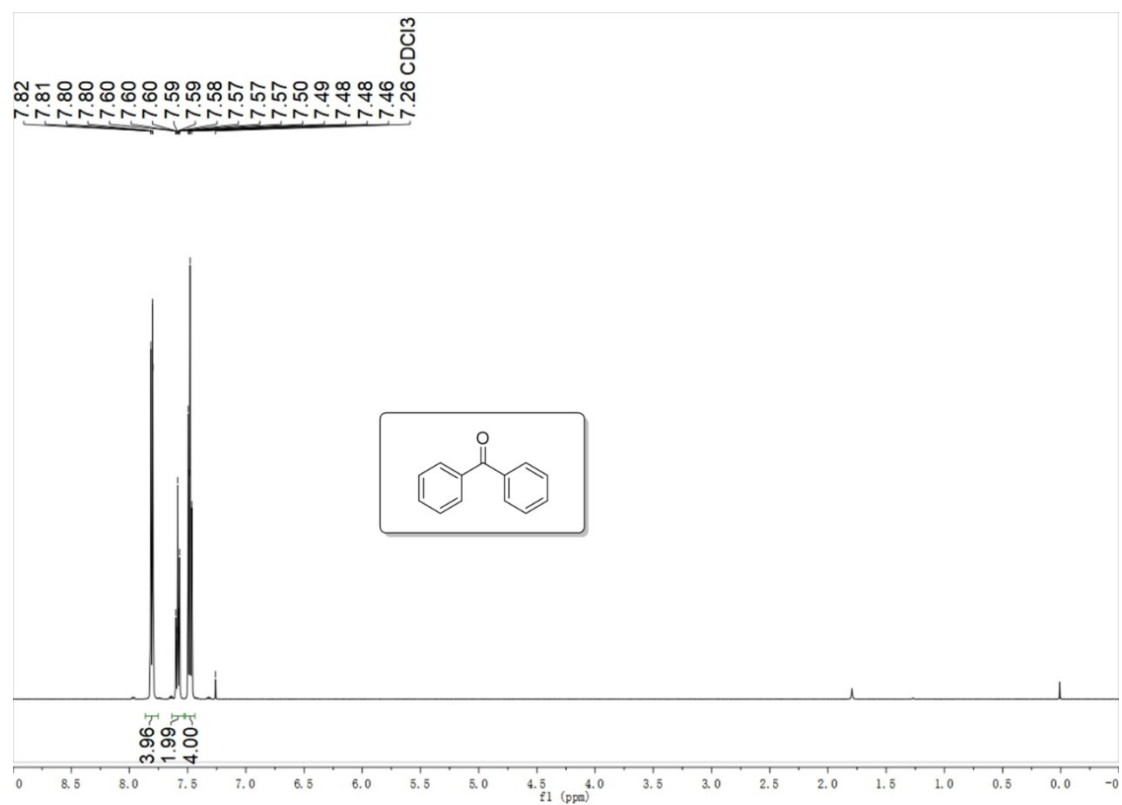
# 4'-Iodoacetophenone (**2f**)



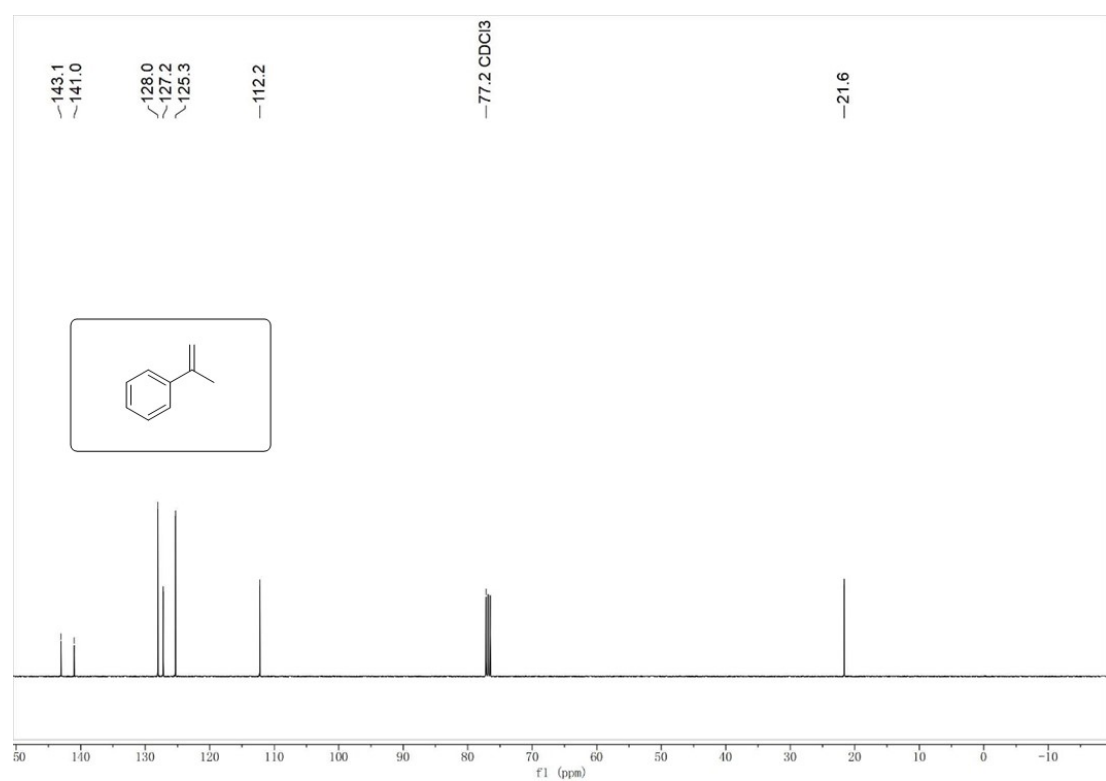
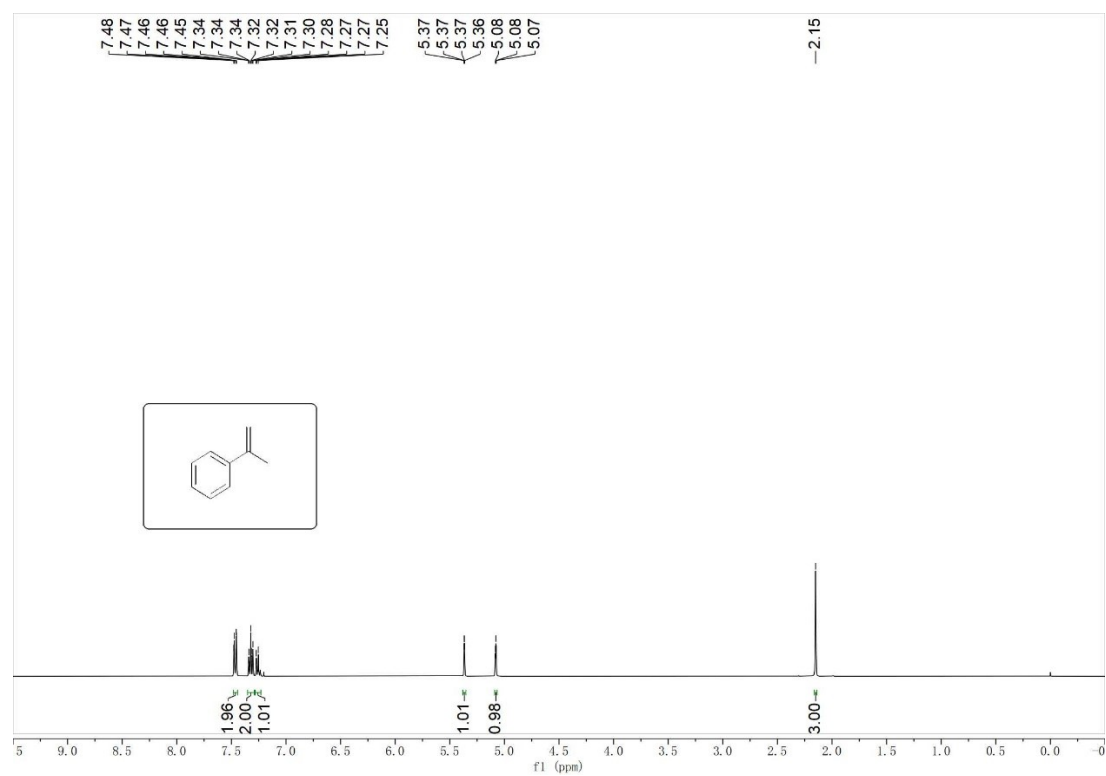
2,3-Dihydro-1*H*-inden-1-one (**2g**)



# Benzophenone (**2h**)



# $\alpha$ -Methyl styrene (AMS)



## 7. Supplementary References

- S1. Kresse; G. Efficient iterative schemes for ab Initio Total-Energy Calculations Using a Plane-Wave Basis Set. *Phys. Rev. B* **1996**, *54*, 11169-11186.
- S2. Perdew, J. P., Burke, K. & Ernzerhof, M. Generalized Gradient Approximation Made Simple. *Phys. Rev. Lett.* **1996**, *77*, 3865.
- S3. Kresse, G., Joubert, D. From Ultrasoft Pseudopotentials to the Projector Augmented-Wave Method. *Phys. Rev. B* **1999**, *59*, 1758.
- S4. Grimme, S., Antony, J., Ehrlich, S. & Krieg, H. A Consistent and Accurate ab Initio Parametrization of Density Functional Dispersion Correction (DFT-D) for the 94 Elements H-Pu. *J. Chem. Phys.* **2020**, *132*, 154104.
- S5. Zhu, H. F.; Zhao, J. N.; Yu, Z. Y.; Li, J. N.; Ma, C. F.; Sun, H. N.; Wu, Y. F.; Meng, Q. W. Visible Light-Driven Sandwich-Like g-C<sub>3</sub>N<sub>4</sub>-Catalyzed Oxidation to Produce Cumene Hydroperoxide. *Ind. Eng. Chem. Res.* **2023**, *62*, 8253–8268.
- S6. Chen, Z. C.; Deng, Y. C.; Yang, G. X.; Zhu, Y. N.; Zhang, Q.; Liu, Z. T.; Y. H.; Cao, Peng, F. Understanding of Cumene Oxidation Catalyzed by Metal-Nitrogen-Carbon through Theoretical Simulations and Kinetic Validation. *ACS. Sustain. Chem. Eng.* **2023**, *11*, 5773–5781.
- S7. Deng, Y. C.; Chen, Z. C.; Huang, J. N.; Yang, G. X.; Zhang, Q.; Liu, Z. L.; Cao, Y. H.; Peng, F. MnO<sub>2</sub> Nanoparticles Supported on CNTs for Cumene Oxidation: Synergistic Effect and Kinetic Modelling. *Chem. Eng. J.* **2022**, *444*, 136666.
- S8. Chen, Z. C.; Li, Y. H.; Cao, Y. H.; Zhang, Q.; Yu, H.; Peng, F. Inhibitory Effect of Zn<sup>2+</sup> on the Chain-Initiation Process of Cumene Oxidation. *Int.J. Quantum.Chem.* **2021**, *121*, e26780.
- S9. G. X. Zhang, Z. N. Zhang, R. Zeng, Photoinduced FeCl<sub>3</sub>-Catalyzed Alkyl Aromatics Oxidation toward Degradation of Polystyrene at Room Temperature. *Chin. J. Chem.* **2021**, *39*, 3225-3230.
- S10. Shen, H. M.; Hu, M. Y.; Liu, L.; Qi, B.; Ye, H. L.; She, Y. B. Efficient and Selective Oxidation of Tertiary Benzylic C-H Bonds with O<sub>2</sub> Catalyzed by

- Metalloporphyrins under Mild and Solvent-Free Conditions. *Appl. Catal. A, Gen.* **2020**, *599*, 117599.
- S11. Inoa, J.; Patel, M.; Dominici, G.; Eldabagh, R.; Patel, A.; Lee, J.; Xing, Y. L. Benzylic Hydroperoxidation via Visible-Light Induced Csp<sup>3</sup>-H Activation. *J. Org. Chem.* **2020**, *85*, 6181–6187.
- S12. Nowacka, A.; Briantais, P.; Prestipinob, C.; Xamena, F. X. L. Selective Aerobic Oxidation of Cumene to Cumene Hydroperoxide over Mono- and Bimetallic Trimesate Metal-Organic Frameworks Prepared by a Facile “Green” Aqueous Synthesis. *ACS. Sustain. Chem. Eng.* **2019**, *7*, 7708–7715.
- S13. Maurya, M. R.; Kumar, U.; Manikandan, P. Synthesis and Characterization of Polymer-Anchored Oxidovanadium (IV) Complexes and Their Use for The Oxidation of Styrene and Cumene. *Eur. J. Inorg. Chem.* **2007**, *16*, 2303–2314.
- S14. Liu, W. G.; Zhang, L. L.; Liu, X.; Liu, X. Y.; Yang, X. F.; Miao, S.; Wang, W. T.; Wang, A. Q.; Zhang, T. Discriminating Catalytically Active FeN<sub>x</sub> Species of Atomically Dispersed Fe-N-C Catalyst for Selective Oxidation of the C-H Bond. *J. Am. Chem. Soc.* **2017**, *139*, 10790–10798.
- S15. Liu, H. S.; Wang, K. J.; Cao, X. Y.; Su, J. X.; Gu, Z. G. A New Highly Active La<sub>2</sub>O<sub>3</sub>-CuO-MgO Catalyst for The Synthesis of Cumyl Peroxide by Catalytic Oxidation *RSC Adv.* **2021**, *11*, 12532–12542.
- S16. Kasperczyk, K.; Orlńska, B.; Zawadiak, J. Aerobic Oxidation of Cumene Catalyzed by 4-Alkyloxycarbonyl-N-Hydroxyphthalimide. *Cent. Eur. J. Chem.* **2014**, *12*, 1176-1182.
- S17. Mu, C. L.; Huang, K. T.; Cheng, T. Y.; Wang, H. J.; Yu, H.; Peng, F. Ni Foams Decorated with Carbon Nanotubes as Catalytic Stirrers for Aerobic Oxidation of Cumene. *Chem. Eng. J.* **2016**, *306*, 806–815.
- S18. Wang, F. F.; Jia, S. Y.; Li, D. L.; Yu, B.; Zhang, L. W.; Y. Liu, Han, X.; Zhang, R.; Wu, S. H. Self-Template Synthesis of CuO@Cu<sub>3</sub>(BTC)<sub>2</sub> Composite and its Application in Cumene Oxidation. *Mate. Lett.* **2016**, *164*, 72–75.

- S19. Xu, S.; Zhang, J.; Chen, B. H.; Lei, Z. G. Process Intensification on the Selective Catalytic Oxidation of Cumene with Ionic Liquids. *Chem. Eng. Process.* **2018**, *130*, 88–92.
- S20. Wang, M.; Wen, J. L.; Huang, Y. H.; Hu, P. Selective Degradation of Styrene-Related Plastics Catalyzed by Iron under Visible Light. *Chem Sus Chem.* **2021**, *14*, 5049–5056.
- S21. Charles-Oneil L. Crites; Geniece L. Hallett-Tapley; Mathieu Frenette; María Gonzalez-Bejar'; J. C. Netto-Ferreira; J. C. Scaiano. Insights into the Mechanism of Cumene Peroxidation Using Supported Gold and Silver Nanoparticles. *ACS Catal.* **2013**, *3*, 2062–2071.
- S22. Chen, Z. C.; Li, Y. H.; Cao, Y. H.; Zhao, Q.; Yu, H.; Peng, F. *Int. J. Quantum Chem.* **2021**, e26780.
- S23. Gao, Y. J.; Hu, G.; Zhong, J.; Shi, Z. J.; Zhu, Y. S.; Su, D. S.; Wang, J. G.; Bao, X. H.; Ma, D. Nitrogen-Doped sp<sup>2</sup>-Hybridized Carbon as a Superior Catalyst for Selective Oxidation. *Angew. Chem. Int. Ed.* **2013**, *52*, 2109-2113.
- S24. Zhou, A.; Huang, J.; Zhao, C.; Fan, Y.; Qin, J.; Chen, Q.; He, M.; Zhou, W. A Simple and Convenient Strategy for the Oxidation of C(sp<sup>3</sup>)–H Bonds Based on  $\gamma$ -Valerolactone. *Green Chem.* **2024**, *26*, 353-361.